

1 **Landscape response to tectonic deformation and cyclic climate change since ca. 800 ka**  
2 **in the southern Central Andes**

3

4 Elizabeth N. Orr<sup>1,2\*</sup>, Taylor F. Schildgen<sup>1,3</sup>, Stefanie Tofelde<sup>4</sup>, Hella Wittmann<sup>1</sup> and Ricardo N.  
5 Alonso<sup>5</sup>

6

7 1: GFZ German Research Centre for Geosciences, Telegrafenberg, 14473 Potsdam, Germany

8 2: Department of Geography, Durham University, Durham, DH1 3LE, United Kingdom

9 3: Institute for Geosciences, University of Potsdam, Karl-Liebknecht-Str. 24-25, 14476 Potsdam, Germany

10 4: Institute of Geological Sciences, Freie Universität Berlin, 12249 Berlin, Germany

11 5: Facultad de Ciencias Naturales, Universidad Nacional de Salta, Salta, 4400 Argentina

12 \*Corresponding author: Elizabeth N. Orr (elizabeth.orr2@durham.ac.uk)

13

14 **Abstract**

15 Theory suggests that the response time of alluvial channel long-profiles to perturbations in climate is  
16 related to the magnitude of the forcing and the length of the system. Shorter systems may record a  
17 higher frequency of forcing compared to longer systems. Empirical field evidence that system length  
18 plays a role in the climate periodicity preserved within the sedimentary record is, however, sparse. The  
19 Toro Basin in the Eastern Cordillera of NW Argentina provides an opportunity to test these theoretical  
20 relationships as this single source-to-sink system contains a range of sediment deposits, located at  
21 varying distances from the source. A suite of eight alluvial fan deposits is preserved along the western  
22 flanks of the Sierra de Pascha. Farther downstream, a flight of cut-and-fill terraces have been linked to  
23 eccentricity-driven (100-kyr) climate cycles since ca. 500 ka. We applied cosmogenic radionuclide  
24 (<sup>10</sup>Be) exposure dating to the fan surfaces to explore (1) how channel responses to external perturbations  
25 may or may not propagate downstream, and (2) the differences in landscape response to forcing  
26 frequency as a function of channel length. We identified two generations of fan surfaces: the first (G1)  
27 records surface activity and abandonment between ca. 800 and 500 ka and the second (G2) within the  
28 last 100 kyr. G1 fans record a prolonged phase of net incision, which has been recognised throughout  
29 the Central Andes, and was likely triggered by enhanced 100-kyr global glacial cycles following the  
30 Mid-Pleistocene Transition. Relative fan surface stability followed, while 100-kyr cut-and-fill cycles  
31 occurred downstream, suggesting a disconnect in behaviour between the two channel reaches. G2 fans  
32 record higher frequency climate forcing, possibly the result of precessional forcing of climate (ca.  
33 21/40-kyr timescales). The lack of a high-frequency signal farther downstream provides field support  
34 for theoretical predictions of a filtering of high-frequency climate forcing with increasing channel  
35 length. We show that multiple climate periodicities can be preserved within the sedimentary record of  
36 a single basin. Differences in the timing of alluvial fan and fluvial terrace development in the Toro  
37 Basin appear to be associated with how channel length affects fluvial response times to climate forcing  
38 as well as local controls on net incision, such as tectonic deformation.

## 39 **Plain Language Summary**

40 Fluvial terraces and alluvial fans in the Toro Basin, NW Argentina record river evolution and global  
41 climate cycles over time. Landform dating reveals lower-frequency climate cycles (100-kyr) preserved  
42 downstream and higher-frequency cycles (21/40-kyr) upstream, supporting theoretical predications that  
43 longer rivers filter out higher-frequency climate signals. This finding improves our understanding of  
44 the spatial distribution of sedimentary paleoclimate records within landscapes.

45

46

### 47 **1. Introduction**

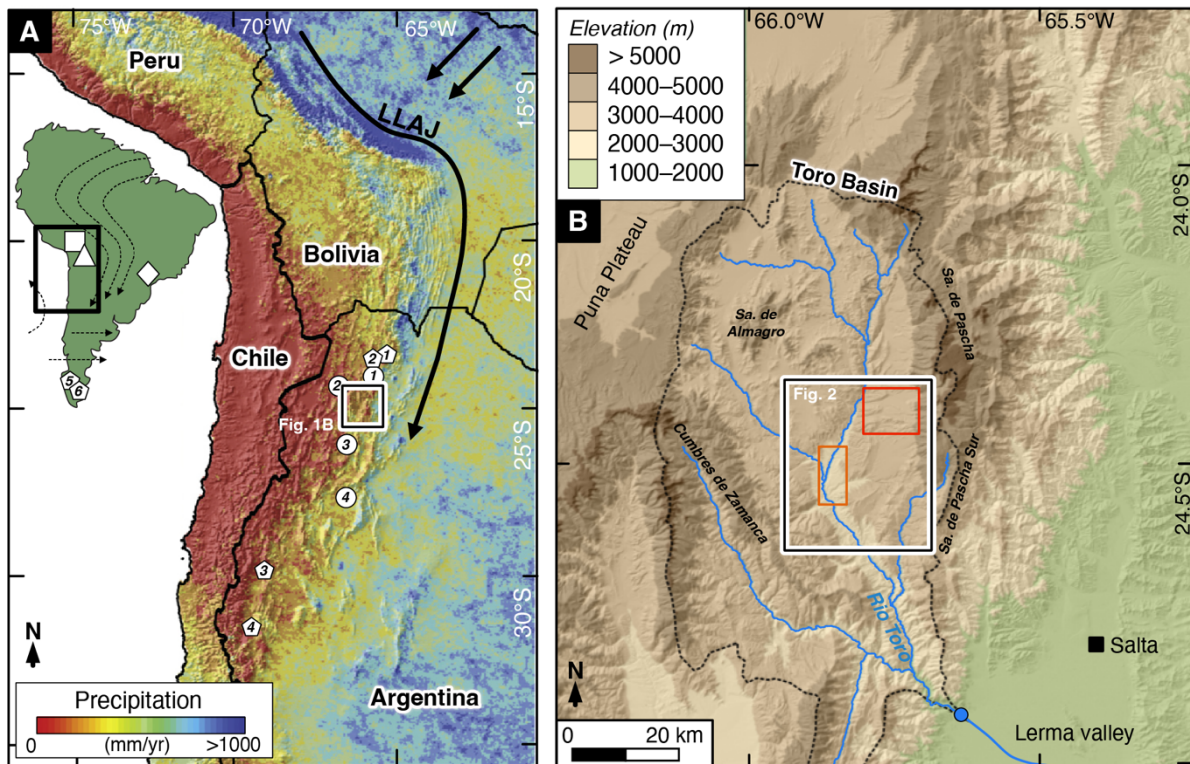
48

49 Fluvial landforms, sediment deposits and the channel form of alluvial systems can be used to reveal  
50 landscape response to past environmental change (Castelltort and Van Den Driessche, 2003, Godard et  
51 al., 2013; Dey et al., 2016; Romans et al., 2016; Mescolotti et al., 2021). Alluvial channels respond to  
52 climate or tectonic driven changes in water discharge, sediment discharge, or base level elevation by  
53 adjusting at least one of their characteristics: bed slope, channel width, channel depth, sediment  
54 transport rates or grain-size distribution (Mackin 1948; Savi et al., 2020). We observe this channel  
55 adjustment via sediment aggradation or incision events, which modify channel bed elevations (Howard,  
56 1982; van den Berg et al., 2008; Wickert and Schildgen, 2019; Tofelde et al., 2019). Fluvial landforms  
57 such as terraces and alluvial fans, which develop along these channels because of this aggradation or  
58 incision, can provide a useful record of how the alluvial-channel system has evolved over time (Rohais  
59 et al., 2012; Armitage et al., 2013; Kober et al., 2013; Counts et al., 2015; Mather et al., 2017; Tofelde  
60 et al., 2021).

61

62 Theory suggests that the time required for an alluvial-channel long profile to adjust to a change in  
63 climate forcing (response time) varies with the magnitude and type of the forcing (sediment supply  
64 versus water supply) and the length of the system; shorter systems respond faster and, hence, may record  
65 a higher frequency of forcing compared to longer systems (Paola et al., 1992; Castelltort and Van Den  
66 Driessche, 2003; Godard et al., 2013; McNab et al., 2023). The length scale over which periodic forcing  
67 delivered at the channel head affects the channel long profile is proportional to the square root of the  
68 period of the forcing (Paola et al., 1992), which means that higher frequency forcing is filtered out with  
69 distance downstream. Evidence of this relationship is preserved in several sedimentary basins in the  
70 Central Andes. Tributary catchments of the Humahuaca Basin (23°S) retain late Quaternary fluvial  
71 deposits between 10 and 100 km downstream from the basin headwaters, which record precessional (21  
72 kyr) cycles in aggradation and incision (Schildgen et al., 2016). In the Toro Basin (24.5°S), a flight of  
73 fluvial cut-and-fill terraces with periodicity of 100-kyr has been linked to eccentricity-driven climate  
74 change (Tofelde et al., 2017). These terraces have an upstream channel length of ~60–80 km. Pliocene-

75 Late Pleistocene sediment deposits are preserved ~140–160 km downstream from the headwaters of  
 76 the Iruya Basin (22°S) of the northern Central Andes and record long eccentricity (400-kyr) cycles  
 77 (Fisher et al., 2023). Crucially, only a single climate periodicity has been recorded in each these basins  
 78 to date. To further test this theoretical relationship between climate periodicity and system length, we  
 79 aim to investigate whether multiple periodicities can be preserved within a single basin, and if this is  
 80 the case, whether higher frequency climate forcing is only observed in the uppermost reaches of the  
 81 basin.  
 82



83 **Figure 1.** Overview of the topography, rainfall and moisture transport of the Central Andes. A) TRMM2B31 (Tropical Rainfall  
 84 Measuring Mission) rainfall map (Bookhagen and Strecker, 2008). Moisture is transported (black arrows) from Atlantic  
 85 sources during the SASM (South American Summer Monsoon) by the Low-Level Andean Jet (LLAJ; Vera et al., 2006). The  
 86 Toro Basin is outlined by the white-black bordered box. Circle symbols denote regional glacial record locations: (1) Nevado  
 87 de Chañi (24.0°S, 65.7°W; Martini et al., 2017), (2) Quevar Volcano (24.4°S, 66.8°W; Luna et al., 2018), (3) Sierra de Quilmes  
 88 (26.2°S, 66.2°W; Zech et al., 2017) and the (4) Sierra de Aconquija (27.2°S, 66.1°W; D’Arcy et al., 2019a). Pentagon symbols  
 89 denote Mid Pleistocene Transition (MPT) geomorphic record locations: (1) Casa Grande Basin (23°S, 66.5°W; Pingel et al.,  
 90 2019b), (2) Salinas Grandes Basin (23.5°S, 66°W; Pingel et al., 2019b), (3) Iglesia Basin (30.5°S, 69°W; Terrizzano et al.,  
 91 2017), (4) Calingasta Basin (32°S, 69.5°W; Peri et al., 2022), (5) Río Deseado (47°S, 72°W; Tobal et al., 2021), (6) Río Santa  
 92 Cruz (50°S, 73°W; Milanez Fernandes, 2023). Inset map of South America indicates Fig. 1A extent and the location of the  
 93 Lake Titicaca (square symbol; Fritz et al., 2007), Salar de Uyuni (triangle symbol; Baker et al., 2001) and Botuverá Cave  
 94 (diamond symbol; Wang et al., 2007) paleoenvironmental records. Dashed arrows outline the moisture-bearing low-level  
 95 airflow patterns for South America which are deflected by the Andean topography. B) Topography of the Toro Basin (ca. 4000  
 96 km<sup>2</sup>, 1500-5900 m asl) from 12-m resolution TanDEM-X (10-m vertical resolution) elevation data. Basin outlined by dashed  
 97 black line. Upper basin delineated by white-black bordered rectangle (see Fig. 2). Toro alluvial fans and fluvial terraces  
 98 outlined by red and orange rectangles, respectively. Basin outlet and start of long profile in Fig. 2 is shown by blue circle. Sa.  
 99 – Sierra.

100  
 101  
 102 Approximately 30 km upstream of the 100-kyr cut-and fill terraces in the Toro Basin is a suite of well-  
 103 preserved alluvial fan surfaces which extend from tributary catchments that drain the Sierra de Pascha  
 104 (Fig. 1). There is limited evidence of sediment storage in these tributary catchments en route to the fans.

105 With an upstream channel length of ~10 km, this fan record may capture geomorphic change linked to  
106 a higher frequency climate forcing than the downstream terraces. The Toro Basin alluvial-channel  
107 system therefore allows us to explore (1) how channel responses to external perturbations may or may  
108 not propagate downstream, and (2) the differences in landscape response to forcing frequency as a  
109 function of channel length when comparing the upper basin alluvial fan deposits with the lower basin  
110 terrace sequence.

111

112 To address these aims, we dated the suite of fan surfaces in the upper Toro Basin using *in situ*-<sup>10</sup>Be  
113 cosmogenic radionuclide (CRN) dating. We used our new Toro fan chronostratigraphy in conjunction  
114 with the fluvial terrace record of Tofelde et al. (2017) to further characterise the evolution of the Toro  
115 Basin over the last million years.

116

## 117 **2. Regional setting**

118

119 The Toro Basin (24.5°S) is an intermontane basin in the Eastern Cordillera of NW Argentina, located  
120 between the high elevation Puna Plateau to the west and the low elevation Andean foreland to the east  
121 (Fig. 1). The mainly gravel-bedded Río Toro flows predominantly south from the low relief upper  
122 reaches of the basin with thick successions of preserved sediment, which are the focus of this study  
123 (referred to as the upper Toro Basin herein), through a steep bedrock gorge, before draining into the  
124 Cabra Corral reservoir in the Lerma valley (Marrett and Strecker 2000). The diffuse shifts in channel  
125 steepness along its course are characteristic of arid, tectonically active landscapes with mechanically  
126 strong basement rocks (Fig. 2B, C) (Bernard et al., 2019, Zondervan et al., 2020; Seagren and  
127 Schoenbohm, 2021).

128

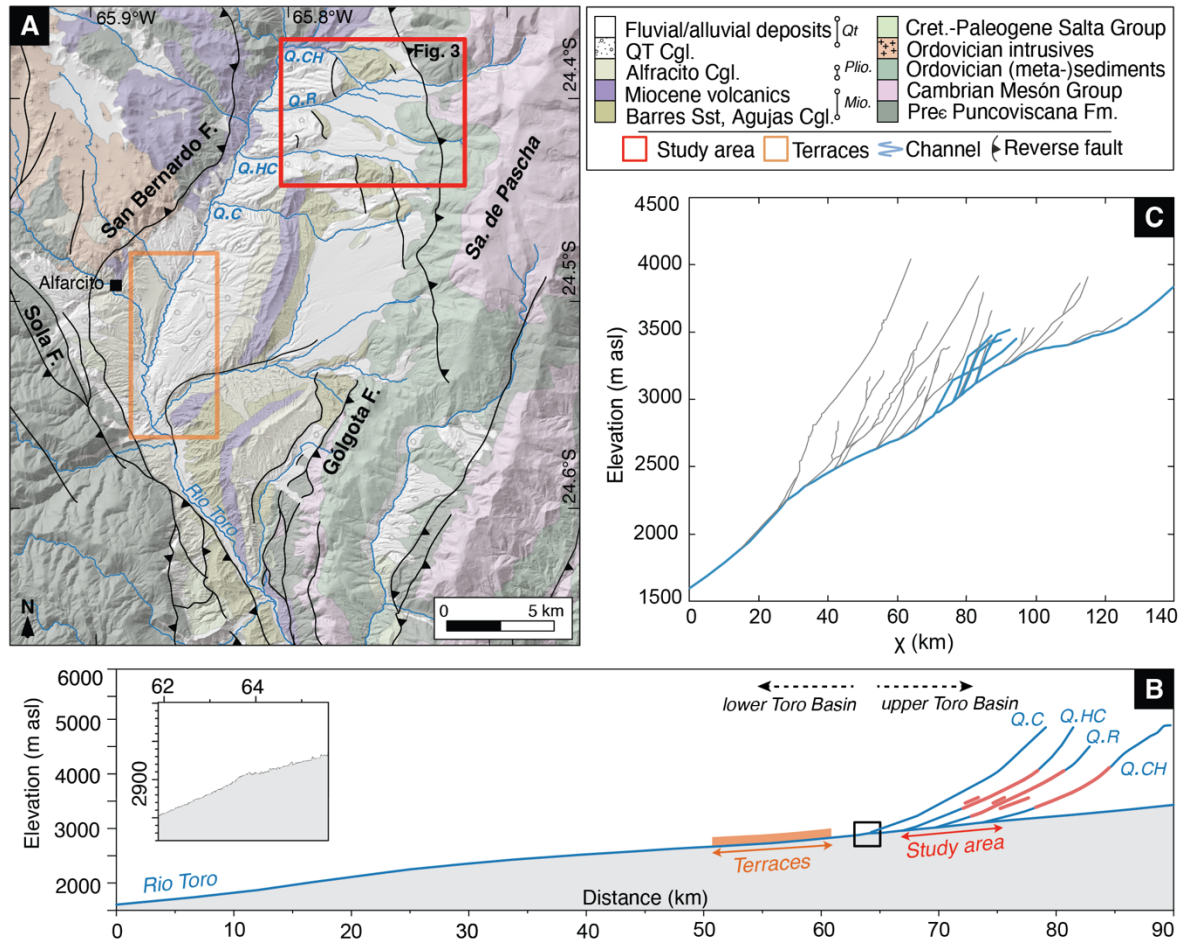
### 129 **2.1 Geology and tectonic setting**

130 The upper Toro Basin is confined by three reverse-fault bounded basement ranges: 1) the Cumbres de  
131 Zamaca bounded by the west-dipping Solá Fault in the west, 2) the Sierra de Almagro bounded by the  
132 northwest-dipping San Bernardo fault in the north, and 3) the Sierra de Pascha Ranges and the east-  
133 dipping Gólgota Fault in the east (Alonso 1992; Marrett and Strecker 2000) (Fig. 1, 2). The Solá fault  
134 has been active since at least the Late Miocene, and tectonic deformation from the Miocene to mid-  
135 Pleistocene has been recorded along the San Bernardo and Gólgota faults (Marrett and Strecker 2000;  
136 DeCelles et al., 2011; Pearson et al., 2013; Pingel et al., 2020). The Gólgota fault reactivated after ca.  
137 0.98 Ma (Hilley and Strecker 2005).

138

139 This study focuses on a suite of fans that emerge from the tributary catchments of the Sierra de Pascha  
140 and are located ~30 km upstream from the cut-and-fill terraces recording 100-kyr climate cyclicity  
141 described by Tofelde et al. (2017). The Pascha Ranges are characterised by meta-sediments of the Late

142 Proterozoic-Cambrian Puncoviscana Formation and quartzites and shales of the Cambrian Mesón  
 143 Group (Schwab and Schafer 1976; García et al., 2013). Long term rock-uplift rates based on structural  
 144 reconstructions range between 0.4 and 0.6 mm/yr (Hilley and Strecker 2005).  
 145



146  
 147 **Figure 2.** Geology and topography of the upper Toro Basin. A) Geologic map with the alluvial fan sequence location (our  
 148 study area, Fig. 3) and cut-and-fill terraces described by Tofelde et al. (2017) outlined by red and orange rectangles  
 149 respectively. Other terraces extend discontinuously along the basin's channel length but remain undated. Map adapted from  
 150 Segemar 250k geological maps and Pingel et al. (2020). Abbreviations: Sa. – Sierra, F – Fault, Q.CH – Quebrada (mountain  
 151 stream) Chacra Huaico, Q.R – Quebrada Rosal, Q. HC – Quebrada Huasa Ciénaga, Q.C – Quebrada del Chorro, Q.Ca –  
 152 Quebrada Carachi, Fm – Formation, Cgl – Conglomerates, Sst – Sandstone. B) Long profile of Toro Basin with tributary  
 153 profiles of upper basin study area. Upper and lower basin reaches are indicated by dashed arrows. Full basin profile extracted  
 154 from fluvial network outlined in Fig. 1. Alluvial fan and terrace surfaces are projected onto profiles. Inset: Higher resolution  
 155 plot of proposed knickzone at confluence between the Río Toro and Quebrada del Chorro (outlined in main plot by black box).  
 156 C) Chi-plot of all channels with a minimum drainage area of 1 km<sup>2</sup> within the Toro basin using a reference concavity index of  
 157 0.45. Bold lines highlight the main river channel and tributary catchments within our study area.  
 158

159 The Middle Miocene Barres Sandstone and Agujas Conglomerates, interbedded with lava flows, and  
 160 the Pliocene-Pleistocene Alfracito Conglomerates make up the west-tilted strata, which lay between the  
 161 fan deposits and the Río Toro (Fig. 2A; Hilley and Strecker, 2005; Mazzuoli et al., 2008). Resistant  
 162 Barres, Agujas and Alfracito units characterise several erosional surfaces that stand ~700 m above the  
 163 modern river channel. Incision into these tectonically deformed units by tributaries draining the Sierra  
 164 de Pascha is thought to have occurred after 0.98 Ma (Hilley and Strecker, 2005), the age of an

165 intercalated ash unit dated from the uppermost layers of the Alfarcito Conglomerate (Marrett et al.,  
166 1994). Undeformed Quaternary conglomerates (also called ‘Terrace Conglomerates’) and  
167 fluvial/alluvial deposits either mantle or infill this tectonically deformed and eroded palaeotopography  
168 (Fig. 2; Marrett and Strecker, 2000; Hilley and Strecker, 2005). The Río Toro sets the local base level  
169 for the Pascha tributaries today (Tofelde et al., 2017).

170

## 171 **2.2 Climatic setting**

172 Moisture mainly governed by the South American Summer Monsoon (SASM) system is directed by the  
173 Low Level Andean Jet (LLAJ) from the Atlantic Ocean and Amazon Basin to the Central Andes (Vera  
174 et al., 2006; Alonso et al., 2006; Bookhagen and Strecker 2008; Castino et al., 2017). The semi-arid  
175 Toro Basin is located towards the southern limit of this moisture conveyor and receives rainfall that  
176 ranges from ~900 mm/yr at the outlet to < 200 mm/yr in the basin headwaters (Fig. 1; Bookhagen and  
177 Strecker 2008). The Sierra de Pascha acts as an orographic barrier, causing the eastern flanks of the  
178 range to be comparatively wetter than the basin interior. The intensity of the SASM and resultant  
179 moisture supply to the Central Andes has been variable over time (see Baker and Fritz, 2015 for detailed  
180 review). Paleoenvironmental records from Argentina, Chile and Bolivia show that SASM precipitation  
181 has varied with changes in insolation over 19 to 25-kyr (precession) (Godfrey et al., 2003, Fritz et al.,  
182 2004, 2010; Placzek et al., 2006; Bobst et al., 2001) and 100-kyr (eccentricity) (Fritz et al., 2007;  
183 Gosling et al., 2008) cycles. The Central Andes are also subject to increased rainfall during periods of  
184 northern hemispheric cooling, whereby the Atlantic part of the intertropical convergence zone (ITCZ)  
185 is forced southward, bringing moisture with it (Broccoli et al., 2006; Mosblech et al., 2012; Novello et  
186 al., 2017; Crivellari et al., 2018). These cold and wet conditions correlate with phases of glacial advance  
187 and rising lake levels (Haselton et al., 2002; Vizy and Cook, 2007; Martin et al., 2018; Mey et al., 2020).

188

189 Successions of glacial moraines are preserved within the Sierra de Pascha tributary catchments and are  
190 indicative of repeated late Quaternary glaciations (Tofelde et al., 2018). Glacial records proximal to the  
191 Toro Basin (24-27.2°S) underline the sensitivity of Andean glaciers to SASM precipitation intensity  
192 and temperature (Martini et al., 2017; Zech et al., 2017; Luna et al., 2018; D’Arcy et al., 2019a; Mey et  
193 al., 2020). The timing of regional glacial stages is invariably in phase with insolation cycles, periods of  
194 SASM strengthening and/or northern hemispheric events (e.g., Younger Dryas, Last Glacial Maximum)  
195 (D’Arcy et al., 2019a).

196

## 197 **2.3 Basin sediment infilling and incision**

198 Thick successions of sediment, together with subtle knickzones and hairpin turns in the Río Toro reflect  
199 a complex late Cenozoic history of basin filling and evacuation (Strecker et al., 2009; Hain et al., 2011;  
200 Vezzoli et al., 2012; Pingel et al., 2020), base level perturbations and tectonic deformation (Marrett and  
201 Strecker, 2000; Hilley and Strecker, 2005; Tofelde et al., 2017), and drainage reorganization (Seagren

202 and Schoenbohm, 2021; Seagren et al., 2022). Given our interest in the Quaternary deposits of the upper  
203 Toro Basin, we focus our attention on how the basin has evolved over the last one million years.

204

205 After deposition of the Alfarcito conglomerates concluded at ca. 0.98 Ma, the Toro Basin was evacuated  
206 to a base level lower than today (Hilley and Strecker, 2005). Renewed hydrological connectivity  
207 between the Toro Basin and the Lerma Valley likely caused widespread basin sediment evacuation and  
208 incision of the (paleo)topography. Uplift of the Sierra de Pascha Sur also recommenced sometime after  
209 ca. 0.98 Ma (Hilley and Strecker, 2005). The newly uplifted range impeded the delivery of precipitation  
210 to the basin interior, and by ca. 0.8 Ma, the semi-arid conditions of today were established (Kleinert and  
211 Strecker 2001; Strecker et al. 2007; Pingel et al., 2020). The mechanically strong basement rocks, and  
212 a potentially reduced sediment transport capacity, meant that incision was unable to keep pace with the  
213 renewed rock uplift. This forced widespread aggradation and a decrease in relief upstream of the  
214 Gólgota fault, and channel steepening within the bedrock gorge cutting through the Sierra de Pascha  
215 Sur (Fig. 2; Hilley and Strecker, 2005; Strecker et al., 2009; García et al., 2013). External drainage  
216 either became restricted or ceased at this time (Marrett et al. 1994; Hain et al., 2011; Pingel et al.,  
217 2019a). Evidence for a similar sequence of events is seen in the Humahuaca, Casa Grande and  
218 Calchaquí basins (23°S), where renewed range uplift reduced hydrological connectivity and caused  
219 sediment infilling (Robinson et al., 2005; Hain et al., 2011; García et al., 2013; Pingel et al., 2013, 2016,  
220 2019a; Streit et al., 2017; Seagren et al., 2022). Although there are some uncertainties about the exact  
221 timing, connectivity between the Toro Basin and the foreland is thought to have been re-established due  
222 to external base-level change (Seagren and Schoenbohm, 2021).

223

224 The Quaternary “Terrace Conglomerates” were deposited within the Toro Basin starting from ca. 0.94  
225 Ma and are considered part of this phase of uplift-induced basin infilling (Hilley and Strecker, 2005). A  
226 flight of six fluvial terrace levels in the lower basin are preserved between 20 and 200 m above the  
227 modern Río Toro (Fig. 2). Cosmogenic exposure-age dating of terraces, burial dating of the sediments,  
228 and zircon U-Pb ages of intercalated ashes from the terrace levels revealed multiple 100-kyr cut-and-  
229 fill sedimentary cycles starting from ca. 500 ka (Tofelde et al., 2017). The phases of incision correspond  
230 with cold, wet glacial periods, when sediment transport capacity apparently exceeded sediment flux,  
231 whereas aggradation occurred when sediment transport was considerably reduced (Tofelde et al., 2017).  
232 Moreover, the calculated net incision rate through the terrace sequence of 0.4 mm/yr from ca. 500 ka is  
233 consistent with long term rock-uplift rates of the Sierra de Pascha Sur (Hilley and Strecker, 2005).  
234 Tofelde et al. (2017) thus concluded that while the renewed uplift of the Sierra de Pascha Sur helped  
235 initiate the deposition of the Terrace Conglomerates, the periodicity of the cut-and-fill cycles is best  
236 explained by orbitally driven climate forcing, with net incision likely associated with the channel  
237 response to ongoing rock-uplift. Today, catchment-averaged erosion rates for catchments draining the  
238 Sierra de Pascha range between <0.03 and 0.12 mm/yr (Tofelde et al., 2018).

239  
240  
241  
242  
243  
244  
245  
246  
247  
248  
249  
250  
251  
252  
253  
254  
255  
256  
257  
258  
259  
260  
261  
262  
263  
264  
265  
266  
267  
268  
269  
270  
271  
272  
273  
274

### 3. Methodology

To evaluate past channel behaviour and landscape response to climate and/or tectonic forcing for the upper Toro Basin, we applied CRN exposure dating to the suite of fan surfaces along the western front of the Sierra de Pascha (Fig. 1, 2).

Alluvial fan CRN ages record the timing of active sediment deposition or surface stability between periods of channel avulsion and incision (Dühnforth et al., 2007; D’Arcy et al., 2019b), which lead to abandonment of the fan surface. This abandonment can occur due to changes in sediment supply (Brooke et al., 2018; Tofelde et al., 2019), tectonic deformation and base level change (Ganev et al., 2010; Mouslopoulou et al., 2017), climate-induced changes in water discharge (Steffen et al., 2010; Savi et al., 2016) or drainage reorganization (Bufe et al., 2017). Because fan surfaces can remain active for  $10^2$ – $10^5$  years before being incised (Cesta and Ward, 2016; Dühnforth et al., 2017; Ratnayaka et al., 2019; Peri et al., 2022), the age distribution or minimum exposure age of boulders on an alluvial fan surface will not necessarily tightly constrain the timing of abandonment. Instead, the distribution of CRN ages, after excluding clear outliers, more likely reflects phases of fan activity, and at best, provide a minimum age limit for the onset of incision leading to eventual surface abandonment (D’Arcy et al., 2019b).

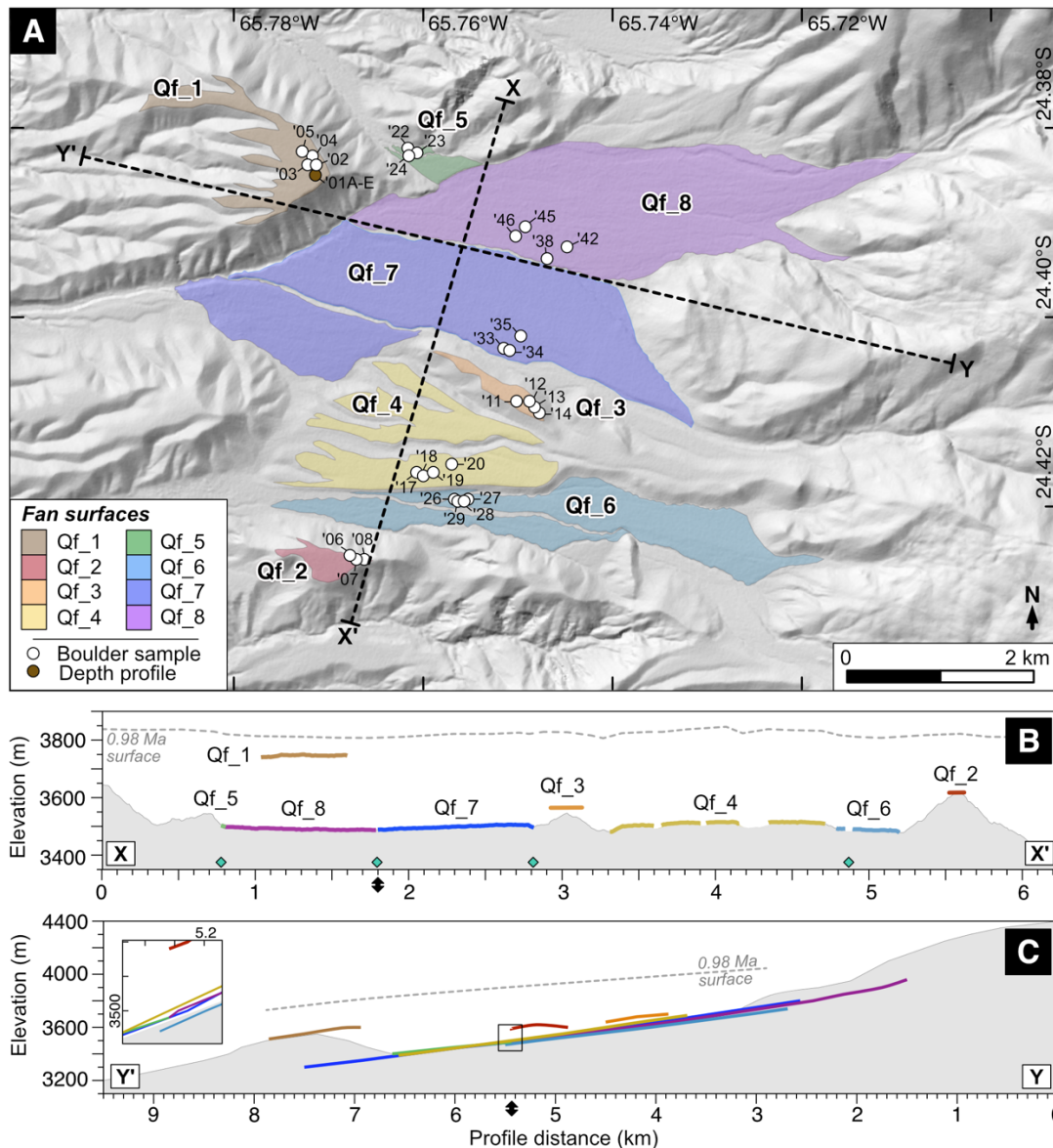
We mapped the upper Toro Basin fans using TanDEM-X (12 m-resolution) data and Google Earth imagery. The stratigraphic relationships among the different fan surfaces were used to inform the cosmogenic radionuclide (CRN) sampling strategy (e.g., McFadden et al., 1989; Hughes et al., 2010; Hedrick et al., 2013).

Supporting topographic, fan and channel data were extracted from the digital elevation model (DEM) using TopoToolbox functions in MATLAB (Schwanghart and Scherler, 2014) and geospatial toolboxes (GRASS, GDAL) in QGIS (geographic information system software). We also compiled a set of climate (Berger and Loutre, 1991; Baker et al., 2001; Imbrie et al., 2006; Fritz et al., 2007; Wang et al., 2007; Lisiecki and Raymo, 2009), paleoenvironmental (Hilley and Strecker, 2005; Tofelde et al., 2017; Pingel et al., 2020), glacial (Martini et al., 2017; Zech et al., 2017; Luna et al., 2018; D’Arcy et al., 2019a; Mey et al., 2020) and geomorphic (Terrizzano et al., 2017; Tofelde et al., 2017; Pingel et al., 2019b; Tobal et al., 2021; Peri et al., 2022; Milanez Fernandes, 2023) records for the Andes to help contextualise our results.

#### 3.1 CRN dating



275 We collected a total of 30 quartzite boulder surface samples from eight fan surfaces (Fig. 3). Between  
 276 three and four boulders were sampled per surface. Each surface was named 'Qf' for 'Quaternary fan',  
 277 followed by a number which referred to its stratigraphic position. For example, Qf\_1 sits ~200 m above  
 278 the modern river channel, and as the highest elevation surface of the study area, it was anticipated to be  
 279 the oldest fan.  
 280



281  
 282 **Figure 3.** Alluvial fan surfaces of the upper basin. A) Hillshade map of the dated fan surfaces with boulder and depth profile  
 283 sampling locations shown. Sample names have been abbreviated (e.g.: TB19\_05: '05). X-X' and Y-Y' linear projection lines  
 284 of Fig. 3B and 3C are represented by dashed black lines. B) Fan sequence stratigraphy shown by fan surfaces projected onto  
 285 X-X'. Qf\_2 and Qf\_3 surface widths are slightly exaggerated to improve visibility. Modern topography shaded in grey. The  
 286 0.98Ma surface (grey dashed line) is modelled from sediment evacuation estimates of Hilley and Strecker (2005). Location of  
 287 active fluvial channels indicated by green diamond symbol. C) Fan surfaces projected onto Y-Y'. Inset plot provides higher  
 288 resolution view of projections (outlined by black rectangle). Projection line intersection is indicated by black double arrow.  
 289

290 Each sampled boulder was embedded within the fan surface, located away from channels, and within  
 291 the distal zone of the landform. This sampling strategy reduced the likelihood that the boulders were

292 sourced from adjacent hillslopes or were part of a depositional event following landform abandonment  
293 (D'Arcy et al., 2019b; Orr et al., 2021). The sampled boulders were the largest, freshest boulders that  
294 we were able to identify within the distal zone. However, we cannot definitively discount the possibility  
295 that the boulders experienced some weathering, surface spallation or fracturing in the past.

296  
297 We removed between 400 and 1000 g of sample from the upper three centimetres of each boulder  
298 surface. The samples were crushed and then sieved to isolate the 250–500  $\mu\text{m}$  grainsize fraction needed  
299 for CRN dating. Sample cleaning, purification, carrier addition, extraction and oxidation of Be, and  
300 target preparation for AMS measurement was conducted in the Helmholtz Laboratory for the  
301 Geochemistry of the Earth Surface (HELGES) at the German Research Centre for Geosciences (GFZ-  
302 Potsdam) using the procedures outlined by von Blanckenburg et al. (2004) and Wittmann et al. (2016).  
303 AMS measurements were completed at the Cologne AMS facility at the University of Cologne,  
304 Germany.

305  
306 Exposure ages derived from *in situ* produced  $^{10}\text{Be}$  concentrations were calculated using the CREp online  
307 calculator (Martin et al., 2017) with the regional reference (SLHL [sea-level, high latitude]) production  
308 rate of 3.74 ( $\pm 0.09$ ) at/ g yr for the high-elevation ( $> 3400$  m asl) Central Andes (Blard et al., 2013;  
309 Kelly et al., 2015; Martin et al., 2015), and the LSD (Lifton-Sato-Dunai) scaling scheme (Lifton et al.,  
310 2014). Further information about the boulder samples, the CRN laboratory procedure, blank ratios, and  
311 age calculation is provided in Supplement 1 and 2.

312  
313 The probabilistic model for inferring the timing of fan surface abandonment from D'Arcy et al. (2019  
314 b) was applied to fans with exposure ages of less than ca. 300 ka. The model uses the exposure ages of  
315 boulders on the fan surface to generate a probability distribution of abandonment ages and a most  
316 probable abandonment age. The modelled abandonment age is based on the premise that an alluvial fan  
317 surface remains active for a period of time that may generate a range of exposure ages exceeding the  
318 uncertainty bounds on any individual age. The calculated abandonment age and its uncertainty is thus  
319 dependent on the youngest measured exposure age, the duration of surface activity, and the number of  
320 samples. For a detailed description of the approach, see D'Arcy et al., (2019b). The model was not  
321 applied to older fan surfaces, which have large age distributions ( $>100$  kyr range) and likely have some  
322 inheritance and/or surface erosion (Phillips et al., 1990; Tobal et al., 2021). Working with chronological  
323 data at this coarse resolution over  $10^5$ – $10^6$ -year timescales means that even the most sophisticated  
324 inheritance/erosion models are limited in their ability to estimate the timing of landform abandonment  
325 (e.g., Prush and Oskin, 2020; Dortch et al., 2022). For the Toro fans where this applies, we use the age  
326 distribution, stratigraphic order of the fans, and youngest exposure age as a guide for the timing of  
327 abandonment.

328

### 329 3.2 <sup>10</sup>Be depth profile

330 To help substantiate our new <sup>10</sup>Be boulder dataset we also resampled the Qf\_1 <sup>10</sup>Be depth profile,  
331 referred to as P6b by Tofelde et al. (2017), and corresponding to their terrace level T6. The original  
332 profile was limited to five samples, which were sampled over relatively broad depth intervals (0–10cm,  
333 18–28 cm, 25–81 cm, 82–164 cm, 164–210 cm). To obtain more highly resolved <sup>10</sup>Be data for this  
334 surface, particularly in the upper 100 cm, five samples of > 65 pebbles each were extracted from the  
335 following depth intervals (cm): 0–10, 20–30, 40–50, 60–70 and 115–125. The pebble samples were  
336 crushed and sieved, and the 500–1000 μm fraction was reserved for CRN dating. Subsequent laboratory  
337 procedures followed that of the boulder samples.

338

339 The Qf\_1 <sup>10</sup>Be depth profile, using combined <sup>10</sup>Be data from this study and from Tofelde et al., (2017),  
340 was used to determine an exposure age using the Hidy et al. (2010) Monte Carlo simulator. Further  
341 details are provided in Supplement 1 and 2.

342

## 343 4. Results

344

345 We use the upper Toro Basin alluvial fan elevations, surface characteristics, and CRN ages to identify  
346 two generations of fan surfaces. The studied fans are predominantly matrix-supported conglomerates  
347 with sub-angular to rounded pebble and cobble clasts. Weathered desert pavements cap many of the fan  
348 surfaces; a layer of finer sands and gravels are overlain by pebbles, cobbles, and boulders (e.g.,  
349 McFadden et al., 1989; Tofelde et al., 2017).

350

351 The Generation 1 (G1) fan surfaces, comprising Qf\_1 through 4, are stratigraphically the highest in the  
352 record and are positioned ~200 to 50 m above the modern river channel(s) (Fig. 3). The fan surfaces are  
353 moderately to highly weathered, with some evidence of surface boulder spallation (Fig. 4). With a few  
354 rare exceptions, the G1 sampled boulders are smaller than those sampled from the lower Generation 2  
355 (G2) surfaces. The G1 and G2 boulders have b-axis lengths which range from 30 to 80 cm and 30 to  
356 140 cm, respectively (Supplement 2). The CRN exposure ages from the G1 surfaces range between ca.  
357 970 and 340 ka (Table 1; Fig. 5, 6).

358

359 G2 is comprised of fans Qf\_5 through 8, which have surfaces within 10 m elevation of the modern  
360 channel(s) (Fig. 3). These moderately weathered surfaces retain debris flow deposits, evidence of past  
361 channel avulsion and sparse human infrastructure (e.g., stone walls). The CRN exposure ages of this  
362 younger fan generation range between ca. 100 and 20 ka, with estimated surface abandonment ages  
363 after ca. 70 ka (Table 1; Fig. 7).

364  
365

**Table 1.** Sample properties, measured *in situ* <sup>10</sup>Be concentrations and calculated exposure ages of each sampled boulder from the Toro fans. Further sample and age calculation details are provided in the Supplement 2 and 3.

Sample	Location			Sample thickness	Shielding correction	Be-10 concentration		Be-10 exposure ages <sup>1</sup>	
	Latitude (°S)	Longitude (°W)	Elevation (m asl)			Concentration (10 <sup>6</sup> at/g SiO <sub>2</sub> )	Uncertainty (10 <sup>6</sup> at/g SiO <sub>2</sub> )	Age (ka)	Uncertainty (ka)
<b>Qf_1</b>									
TB19_02	-24.38492	-65.76890	3556	1	0.990	24.20	0.78	966.63	109.78
TB19_03	-24.38492	-65.76890	3556	1	0.990	16.02	0.52	593.11	59.10
TB19_04	-24.38492	-65.76890	3556	1	0.990	22.33	0.72	884.41	95.34
TB19_05	-24.38492	-65.76890	3556	1	0.990	16.97	0.55	639.17	63.94
<b>Qf_2</b>									
TB19_06	-24.42522	-65.76775	3560	1	0.999	11.36	0.37	391.94	37.91
TB19_07	-24.42566	-65.76682	3570	2	0.999	17.00	0.55	631.77	64.10
TB19_08	-24.42568	-65.76607	3581	2	0.999	10.18	0.33	336.94	33.17
<b>Qf_3</b>									
TB19_11	-24.40882	-65.75023	3644	1	0.998	15.45	0.50	533.56	52.88
TB19_12	-24.40918	-65.74864	3658	3	0.998	18.06	0.59	651.82	66.21
TB19_13	-24.40976	-65.74810	3660	3	0.998	17.77	0.58	634.67	64.63
TB19_14	-24.41011	-65.74773	3673	3	0.998	11.18	0.37	361.38	35.49
<b>Qf_4</b>									
TB19_17	-24.41665	-65.76059	3509	1	0.999	14.73	0.48	548.44	54.60
TB19_18	-24.41675	-65.76000	3512	2	0.999	17.26	0.56	679.67	68.23
TB19_19	-24.41654	-65.75923	3519	3	0.999	19.06	0.61	778.81	79.15
TB19_20	-24.41533	-65.75681	3541	1	0.999	21.41	0.69	847.34	90.30
<b>Qf_5</b>									
TB19_22	-24.38245	-65.76145	3404	2	0.990	2.02	0.07	70.63	6.28
TB19_23	-24.38263	-65.76109	3407	2	0.995	2.34	0.08	82.69	7.35
TB19_24	-24.38275	-65.76144	3405	3	0.995	2.77	0.09	98.81	8.82

**Qf\_6**

TB19_26	-24.41923	-65.75623	3531	2	0.998	2.16	0.07	69.97	6.27
TB19_27	-24.41921	-65.75578	3532	1	0.998	2.52	0.08	81.85	7.31
TB19_28	-24.41924	-65.75569	3541	2	0.998	2.22	0.08	71.11	6.46
TB19_29	-24.41941	-65.75652	3525	3	0.998	2.47	0.08	82.00	7.33

**Qf\_7**

TB19_33	-24.40346	-65.75108	3557	1	0.998	1.22	0.04	38.78	3.46
TB19_34	-24.40371	-65.75107	3555	2	0.998	1.87	0.06	59.28	5.36
TB19_35	-24.40203	-65.74977	3563	3	0.998	2.11	0.07	66.94	6.13

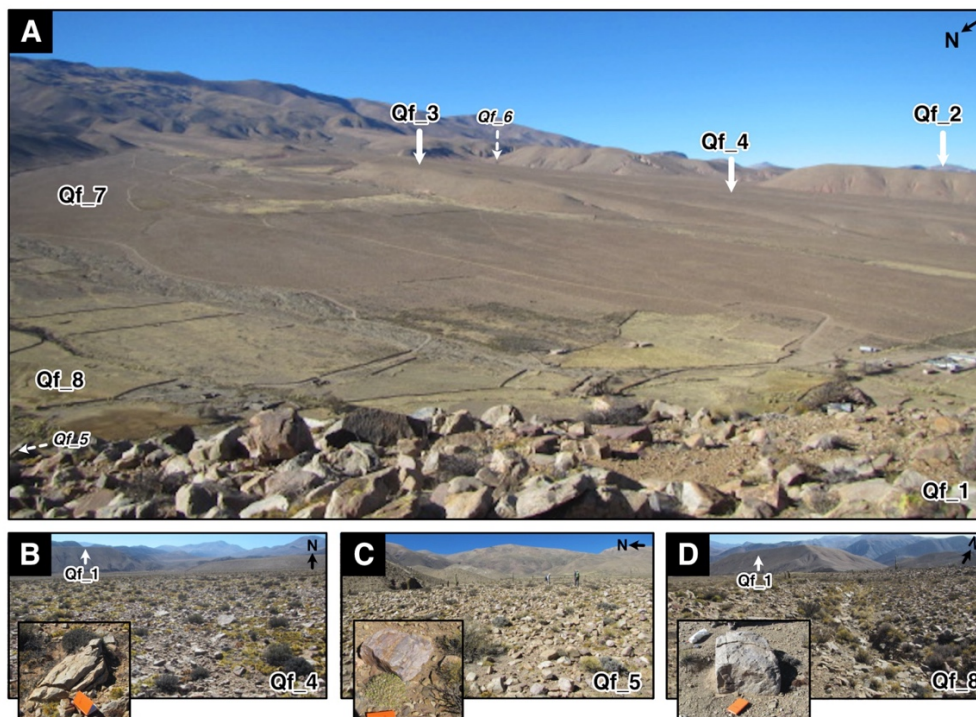
**Qf\_8**

TB19_38	-24.39402	-65.74711	3533	1	0.997	1.43	0.05	44.34	4.08
TB19_42	-24.39275	-65.74500	3553	1	0.997	1.43	0.05	43.65	4.04
TB19_45	-24.39043	-65.74940	3510	1	0.997	0.63	0.02	22.37	1.85
TB19_46	-24.39140	-65.75027	3502	1	0.997	1.44	0.05	45.32	4.212

366  
367  
368

1: LSD scaling scheme (Lifton et al., 2014), ERA40 Atmosphere Model (Uppala et al., 2005), LSD framework for geomagnetic correction (Lifton et al., 2014), Reference (SLHL) production rate:  $3.74 \pm 0.09$  at/g/yr. Sample density:  $2.75 \text{ g cm}^{-3}$ . Erosion:  $0 \text{ mm yr}^{-1}$

369  
370  
371  
372  
373  
374  
375  
376



378

379 **Figure 4.** Images of the alluvial fan sequence of the upper Toro Basin. A) Image taken from Qf\_1 surface (facing SE) with  
 380 fan surfaces labelled. Italicized text with arrows indicates location of surfaces that are not clearly in shot. B) Qf\_4 surface.  
 381 Inset image of sampled boulder TB19\_19. C) Qf\_5 surface. Inset image of sampled boulder TB19\_22. D) Qf\_8 surface. Inset  
 382 image of sampled boulder TB19\_44. Images B–D encompass full age range of sampled surfaces. Further images of the fan  
 383 surfaces and  $^{10}\text{Be}$  samples are provided in Supplement 3.

384

#### 385 4.1 Generation 1

386 Qf\_1 is the highest fan surface of the record (~200 m above the modern channel), which extends from  
 387 the Quebrada Rosal tributary catchment. The fan comprises part of the Quaternary conglomerates,  
 388 which overlie the Barres Sandstone Formation (Fig. 2, 3). The depth profile is composed of four  
 389 sedimentary units that coarsen with depth: silts and fine sands (0–20 cm), fine-coarse sand (20–60 cm),  
 390 coarse sand and gravel (60–180 cm) and gravels (>180 cm). Consistent with the original profile, the  
 391 new  $^{10}\text{Be}$  sample concentrations decrease exponentially with depth (Fig. 5; Table 2). Qf\_1 has a  
 392 Bayesian most-probable exposure age of  $715.8^{+35}_{-217}$  ka ( $2\sigma$  upper age: 750.8 ka,  $2\sigma$  lower age: 498.8  
 393 ka) and  $0.26 \pm 0.42 \times 10^6$  atoms/g of inheritance. Within the simulator, we constrained fan surface erosion  
 394 and inflation by setting the erosion rate to range between -0.02 and 0.2 cm/ka and using maximum and  
 395 minimum erosion thresholds of -10 and 50 cm, respectively. While this modelled exposure age is  
 396 consistent with the age estimated earlier by Tofelde et al. (2017) of  $732^{+53}_{-56}$  ka assuming a stable  
 397 surface, or  $644^{+43}_{-49}$  ka accounting for surface inflation, Tofelde et al. (2017) preferred the exposure  
 398 age they derived from surface pebbles of  $453 \pm 33$  ka.

399

400 The exposure ages of boulder samples TB19\_03 and TB19\_05 are in agreement with the depth profile  
 401 results, yielding exposure ages of  $639.17 \pm 63.94$  and  $593.11 \pm 59.10$  ka ( $2\sigma$  uncertainty). The two

402 remaining boulders (TB19\_02, TB19\_04) yielded older exposure ages of  $966.63 \pm 109.78$  and  $884.41$   
 403  $\pm 95.34$  ka.

404

405 **Table 2.** Sample depths and measured  $^{10}\text{Be}$  concentrations of Qf\_1 depth profile. Fan age calculated with the Hidy  
 406 et al. (2010) Monte Carlo depth profile simulator was  $715.8^{+35}/_{-217}$  ka. Inheritance measured:  $0.26 \pm 0.42 \times 10^6$   
 407 at/g $\text{SiO}_2$ .

Sample <sup>1</sup>	Sample depth		Be-10 concentration	
	Depth (cm)	Uncertainty (cm)	Concentration ( $10^6$ at/g $\text{SiO}_2$ )	Uncertainty ( $10^6$ at/g $\text{SiO}_2$ )
BBC-0	5	5	14.70	0.18
TB19_01A	5	5	14.97	0.48
BBC-1	23	5	11.80	0.11
TB19_01B	25	5	12.14	0.39
TB19_01C	45	5	10.88	0.35
BBC-2	53	28	7.76	0.07
TB19_01D	65	5	8.76	0.28
TB19_01E	120	5	4.94	0.16
BBC-3	123	41	5.21	0.06
BBC-4	187	23	2.30	0.03

408 1: TB19\_01A-E from this study. 'BBC-1-4' from Tofelde et al. (2017).

409

410 Surface Qf\_2, the second highest surface (ca. 130 m above the closest modern channel), also overlies  
 411 the Barres Sandstone and likely extends from the Quebrada Huasa Ciénaga and Quebrada del Chorro  
 412 catchments. CRN exposure ages from three boulders range from  $631.88 \pm 64.10$  to  $336.94 \pm 33.17$  ka.

413

414 The Qf\_3 surface is positioned ca. 60 m above the closest modern channel and extends from the  
 415 Quebrada Rosal tributary catchment. The surface yields three CRN boulder exposure ages that cluster  
 416 between  $651.82 \pm 66.21$  and  $533.56 \pm 52.88$  ka, and one younger age of  $361.38 \pm 35.49$  ka.

417

418 Qf\_4 has a highly dissected fan surface which is the lowest stratigraphically of the G1 fans; the fan is  
 419 positioned ca. 40 m below the Qf\_3 surface and ca. 30 m elevation above the modern channel. Four  
 420 boulder exposure ages range from  $911.61 \pm 100.27$  to  $548.44 \pm 54.60$  ka.

421

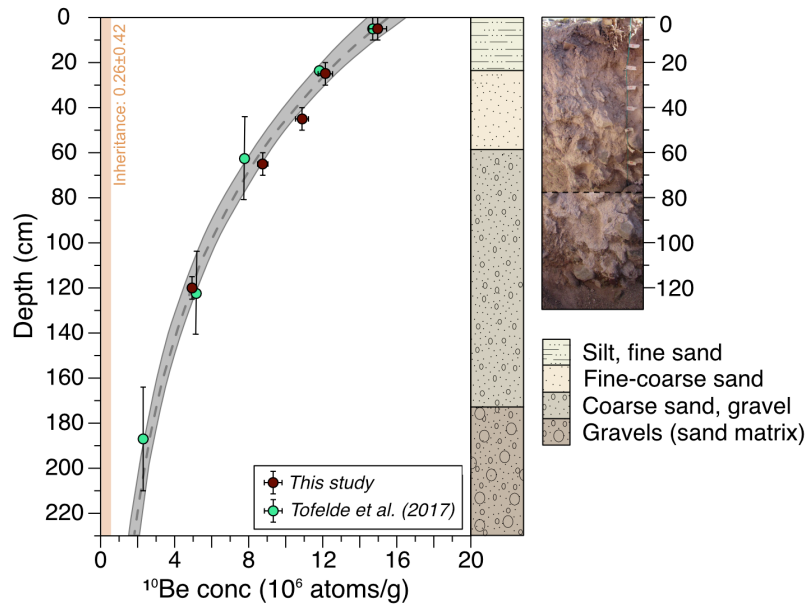
## 422 4.2 Generation 2

423 Qf\_5 is a small G2 surface that sits ca. 10 m above the neighboring Qf\_8 fan. Qf\_5 has three exposure  
 424 ages that range from  $98.81 \pm 8.82$  to  $70.63 \pm 6.28$ ka, with a most probable abandonment age of  $61.8$   
 425  $^{+13.5}/_{-33.6}$  ka (no ages excluded as outliers).

426

427 Qf\_6's surface is characterized by moderately weathered debris flow deposits with clusters and  
 428 elongated ridges of boulders. Exposure ages range between  $82.00 \pm 7.33$  and  $69.97 \pm 6.27$  ka from the

429 four boulders, with an estimated surface abandonment age of  $66.2^{+11.0}/_{-17.5}$  ka (no ages excluded as  
 430 outliers).



431  
 432 **Figure 5.**  $^{10}\text{Be}$  concentration with depth for Qf\_1 profile alongside sedimentary log and stitched field image of the profile pit.  
 433 Each sample was collected over a depth range represented by a vertical error bar. Horizontal error bar represents the  $1\sigma$   
 434 analytical uncertainty for the nuclide concentration. The Hidy et al. (2010) Monte Carlo simulator fit 100,000 curves (grey  
 435 shading) to profile and generated most probable fit (grey dashed line). Modelled inheritance is shown by orange line. \*Profile  
 436 6b data, rather than 6a, from the supplementary materials is used in simulation, due to the mislabelling of the profile in Fig. 4  
 437 of Tofelde et al. (2017).  
 438

439 Despite Qf\_7 being located within 5 m elevation of the youngest G2 fan Qf\_8, this large fan appears  
 440 more weathered than Qf\_8. Qf\_7 has CRN exposure ages of  $66.94 \pm 6.13$ ,  $59.28 \pm 5.35$  and  $38.78 \pm$   
 441  $3.47$  ka. The surface abandonment ages including and excluding the youngest age are  $33.9^{+7.4}/_{-25.1}$  and  
 442  $52.9^{+11.0}/_{-16.3}$  ka, respectively.  
 443

444 Surface Qf\_8 yielded a cluster of older ages that range between  $45.32 \pm 4.2$  and  $43.65 \pm 4.04$  ka and a  
 445 single younger age of  $22.37 \pm 1.83$  ka. Abandonment ages including and excluding the youngest age  
 446 are  $19.4^{+4.1}/_{-19.4}$  and  $42.4^{+6.5}/_{-7.5}$  ka, respectively. The surface is covered with relatively unweathered  
 447 debris flow deposits and large varnish-free boulders.  
 448

## 449 5. Discussion

450  
 451 While there are some nuances to the Toro Basin fan record, our new CRN dataset enables us to identify  
 452 significant phases of net incision since ca. 0.98 Ma, capture the channel response to external forcing  
 453 over a range of timescales and cyclicities, and gain further insight into the late Quaternary evolution of  
 454 the Toro Basin.  
 455



## 456 **5.1 Timing of alluvial fan development and abandonment**

457 CRN age uncertainties on the order of  $10^4$ – $10^5$  years and a wide range of fan exposure age distributions  
458 on individual surfaces present some challenges when interpreting the Toro fan chronostratigraphy,  
459 which is crucial for comparison with potential external forcing conditions. Constraining the geological  
460 uncertainties of the CRN ages, particularly for old fan surfaces, is often challenging (Owen et al., 2014).  
461 For this reason, we use geological, topographic and paleoenvironmental data alongside the  $^{10}\text{Be}$  data to  
462 interpret the alluvial fan record. The coarse resolution of the G1  $^{10}\text{Be}$  record means that while we can  
463 reflect upon long term shifts in channel behaviour for the upper Toro Basin, we must exercise caution  
464 when linking this record to specific forcing or events (Gray et al., 2014; Dühnforth et al., 2017; Orr et  
465 al., 2021). Pairing the  $^{10}\text{Be}$  record with cosmogenic  $^{21}\text{Ne}$  in the future may help to decipher some of the  
466 complexities in the exposure histories of the boulders;  $^{21}\text{Ne}$  is well suited for quantifying long term  
467 landscape change in arid, low erosion environments (Dunai et al., 2005; Ma and Stuart, 2018).

468

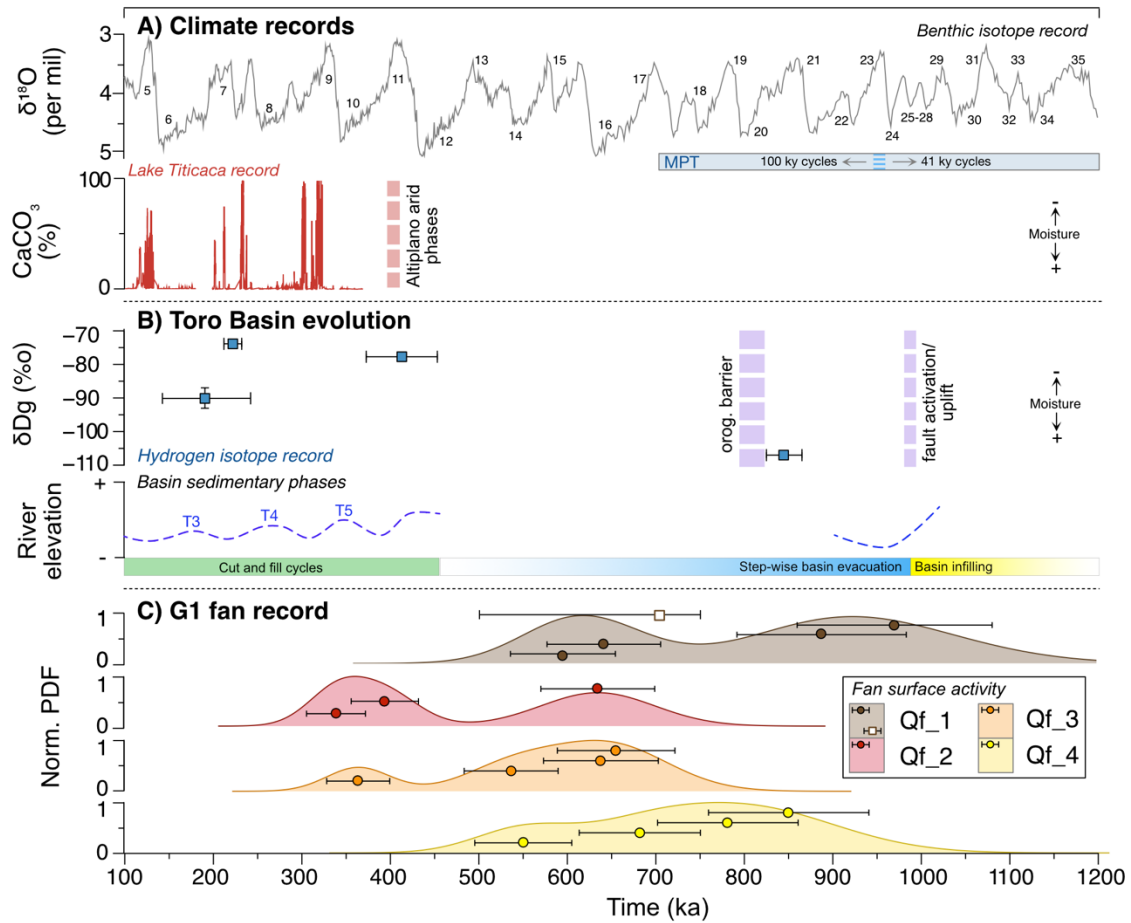
### 469 *5.1.1 Fan Generation 1*

470 The ~200-m elevation difference between the highest and lowest fan surface among Generation 1 means  
471 that the G1 surfaces could not have been active simultaneously (Fig. 6). Substantial inheritance and/or  
472 erosion has therefore likely affected individual boulders from these surfaces and offers one explanation  
473 for the broad spread in ages (>400 kyr) for each.

474

475 Pairing the Qf\_1  $^{10}\text{Be}$  depth profile with the surface boulder exposure ages means that we can more  
476 robustly constrain the oldest phase of fan development within the study area and use it as a benchmark  
477 when evaluating the remainder of the G1 fan record. The most recent phase of Qf\_1 surface activity  
478 and/or stability is constrained by the depth profile data and two boulders to between ca. 750 and 600  
479 ka. In this case, we believe that CRN inheritance may explain why the remaining two boulders  
480 (TB19\_02, TB19\_04) from this surface yield exposure ages that exceed ca. 800 ka. Considering the  
481 whole suite of boulder ages for the G1 fans, which mostly exceed 500 ka, we find it unlikely that the  
482 age of  $453 \pm 33$  ka (based on surface pebbles) originally reported by Tofelde et al. (2017) for Qf\_1 is  
483 correct.

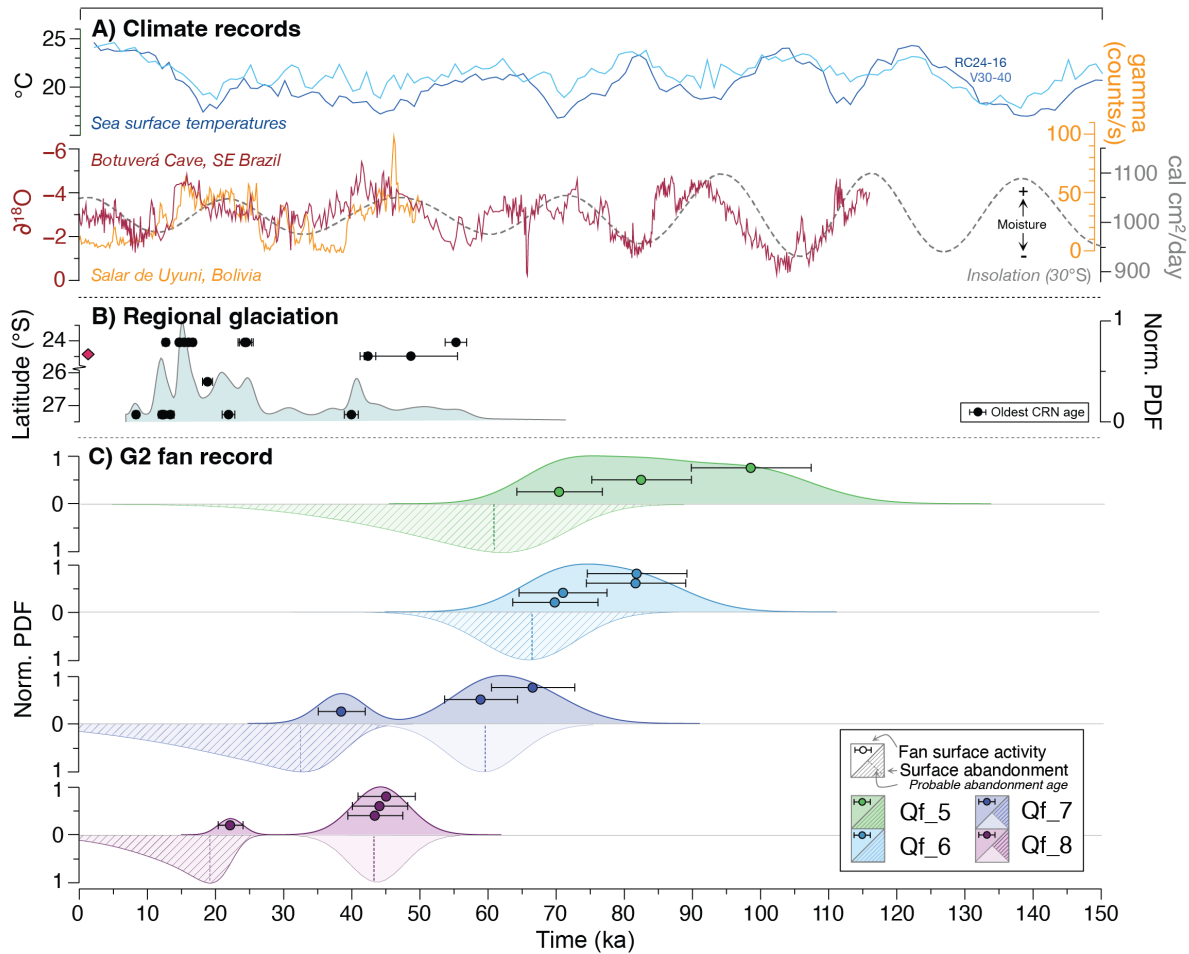
484



485 **Figure 6.** Comparison between the G1 fan  $^{10}\text{Be}$  dataset and records of Toro Basin evolution and climate. A) Benthic isotope  
 486 record (Lisiecki and Raymo 2009) displayed alongside Marine Isotope Stages (MIS) and Mid-Pleistocene Transition labelling  
 487 and the Lake Titicaca sediment core record ( $\text{CaCO}_3$  concentration) from Fritz et al. (2007). B) Toro basin evolution. Climatic  
 488 variability represented by hydrogen isotope record of Pingel et al. (2020). Basin sedimentary and tectonic phases plotted with  
 489 respect to inferred river elevation over time, as observed by this study and described by Hilley and Strecker (2005), Tofelde et  
 490 al. (2017) and Pingel et al. (2020). Fluvial terrace record (T3-6) from Tofelde et al. (2017). C)  $^{10}\text{Be}$  surface boulder ages and  
 491 normalised probability density functions (PDFs) of the G1 surfaces. Horizontal error bars represent the  $1\sigma$  uncertainty for the  
 492 exposure ages. Bayesian modelled surface age of Qf\_1 ( $715.8^{+35}_{-217}$  ka) derived from depth profile (Fig. 5) is denoted by  
 493 square point.  
 494

495 Given the stratigraphic positions of Qf\_2 and Qf\_3, it is unlikely that active streams were present on  
 496 these surfaces after ca. 400 ka. For this reason, we suggest that the younger ages for these surfaces are  
 497 the result of erosion. These surfaces also must be older than surface Qf\_4, which yielded a youngest  
 498 age of ca. 550 ka.

499  
 500 Inheritance also likely explains the old (>750 ka) boulders on Qf\_4, which is stratigraphically younger  
 501 than Qf\_1 and cannot have been active at the same time.



502

503 **Figure 7.** Comparison between the G2 fan <sup>10</sup>Be dataset and regional climate and glacial records. A) Climate records. Sea  
 504 surface temperatures from Imbrie et al. (2006), insolation from Berger and Loutre (1991), Botuverá Cave, SE Brazil  
 505 speleothem record from Wang et al. (2007) and Salar de Uyuni, Bolivia lake record from Baker et al. (2001). B) CRN glacial  
 506 chronologies from the Central Andes (see Fig. 1A for location) : Nevado de Chañi (24°S, 65.7°W, Martini et al., 2017, Mey  
 507 et al., 2020), Quevar Volcano (24.4°S, 66.8°W, Luna et al., 2018), Sierra de Quilmes (26.2°S, 66.2°W, Zech et al., 2017) and  
 508 the Sierra Aconquija (27.2°S, 66.1°W, D’Arcy et al., 2019a). Location of Toro Basin (24.4°S, 66.7°W) is indicated by red  
 509 diamond symbol. C) <sup>10</sup>Be surface boulder ages and normalised probability density functions of the G2 surfaces. Horizontal  
 510 error bars represent the 1σ uncertainty for the exposure ages. Normalised PDF of fan surface abandonment (hashed shading)  
 511 calculated using the D’Arcy et al. (2019b) probabilistic model for fan surface abandonment. Surface abandonment for Qf\_7  
 512 and Qf\_8 without youngest boulder ages (TB19\_33 and TB19\_45, respectively) shown by PDFs with opaque solid shading.  
 513 Most probable abandonment ages denoted with dashed vertical lines- Qf\_5: 61.8<sup>+13.5/-33.6</sup> ka, Qf\_6: 66.2<sup>+11.0/-17.5</sup> ka, Qf\_7: ca.  
 514 33.9<sup>+7.4/-25.1</sup> ka (52.9<sup>+11.0/-16.3</sup> ka), Qf\_8: 19.4<sup>+4.1/-19.4</sup> ka (42.4<sup>+6.5/-7.5</sup> ka).

515

516 Given these complexities in the fan chronostratigraphy, rather than identifying discrete phases of  
 517 aggradation and incision for each fan surface, we suggest that the G1 fan record can instead be used to  
 518 capture an extended phase of net incision within the Sierra de Pascha tributaries. Crucially, this is  
 519 unlikely continuous incision, but rather a phase of net incision, which was punctuated by the formation  
 520 of individual surfaces, possibly controlled by higher frequency climate cyclicity (e.g. 100-kyr). If so,  
 521 this would imply periods of faster incision through the fill. By comparing the G1 fan record with the  
 522 modelled palaeotopography of Hilley and Strecker (2005), we estimate that ~100 m of net incision  
 523 (~0.01 mm/yr) occurred within the upper basin between ca. 0.98 Ma and 800 ka, at which point the  
 524 Qf\_1 surface became active (Fig. 3B, C, Fig. 8). Approximately 200 m of net incision (~0.07 mm/yr)

525 then followed between ca. 800 ka and the complete abandonment of the G1 fans by ca. 500 ka (when  
526 adjusting for age outliers) (Fig. 6), which signals the significant stepwise evacuation of sediment from  
527 the upper Toro Basin at this time.

528

### 529 *5.1.2 Fan Generation 2*

530 The G2 record reveals that after a hiatus in the geomorphic record ca. 500 and 100 ka, fan aggradation  
531 and incision is recorded throughout several of the Sierra de Pascha tributaries (Fig. 8). Rather than  
532 recording continuous fan activity since ca. 110ka, the distribution of ages for G2 instead likely captures  
533 multiple distinct phases of deposition. The G2 fan surfaces have much tighter constrained age  
534 distributions (ca. 21 to 40 kyr) compared to the G1 fans, with two G2 fans showing what may be young  
535 outliers; the boulders are therefore less likely to be affected by inheritance, but the young outliers may  
536 be affected by erosion or tilting by human or animal activity.

537

## 538 **5.2 Drivers of alluvial channel system change and fan/terrace formation**

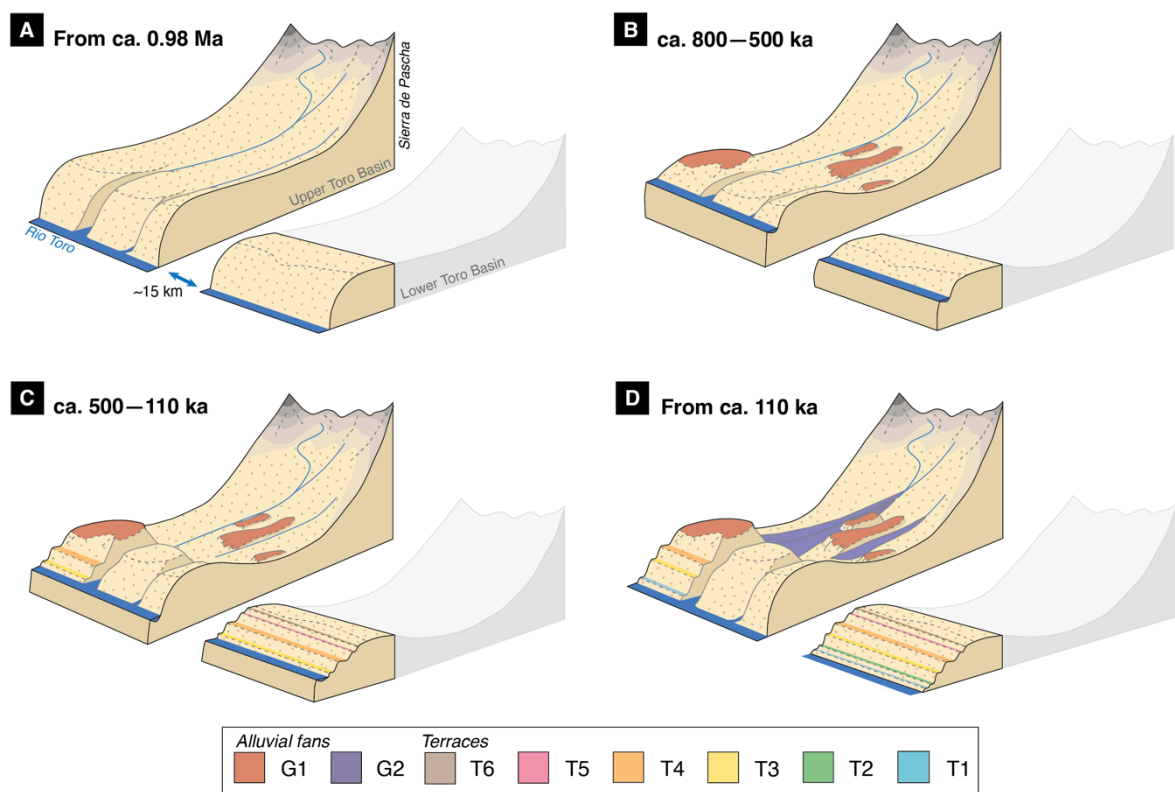
539 Before we can explore some of the possible explanations for the alluvial system change recorded in the  
540 Toro Basin, we must first consider the specific local conditions needed to help explain the G1 (ca. 800  
541 to 500 ka) and G2 (ca. 100 to 20 ka) fan generations in the upper basin, as well as the fluvial terrace  
542 sequence (ca. 370 ka to <75 ka) in the lower basin. Changes in water or sediment discharge, governed  
543 by climate, can affect channel slopes and prompt adjustments to the channel bed elevations through  
544 incision or aggradation (Howard, 1982; Wickert and Schildgen, 2019; Tofelde et al., 2019).  
545 Nevertheless, net incision is essential to preserving the geomorphic record of aggradation-incision  
546 cycles. Otherwise, subsequent aggradational phases are likely to bury earlier landforms. Net incision  
547 can occur through the channel response to ongoing rock uplift or base level fall (Simpson and  
548 Castelltort, 2012), the latter of which may include renewed incision through an aggraded sequence of  
549 sediment downstream. While autogenic processes, such as channel avulsion and meander cut-offs may  
550 also play a role in channel incision and the formation of discrete fan lobes or terraces (Nicholas and  
551 Quine, 2007; Ventra and Nichols, 2014), we consider the scale of channel incision associated with the  
552 features of interest (ranging from ca. 10 to hundreds of meters) is beyond the scope of purely autogenic  
553 behavior. Below, we consider how climate-modulated changes to water and sediment discharge,  
554 together with events that can drive net incision, may have helped to generate, and preserve multiple  
555 generations of fans and terraces within the Toro Basin.

556

### 557 *5.2.1 Fan formation from ca. 800 to 500 ka*

558 The development, entrenchment, and eventual abandonment of the G1 fans could be part of the  
559 landscape response to enhanced rock-uplift of the Sierra de Pascha Sur, starting no later than ca. 800 ka  
560 (Fig. 8) (Clarke et al., 2010; Mather et al., 2017; Mouchené et al., 2017). However, another mechanism  
561 is likely at play because the averages rates of incision between ca. 800 and 500 ka (0.8 mm/yr) as

562 recorded by the G1 fans, exceed the estimated rock uplift rates of 0.4 – 0.6 mm/yr (Hilley and Strecker,  
 563 2005), and tectonic uplift alone is unlikely to be pulsed in a manner that would generate multiple fans.  
 564 More likely, both climate forcing and tectonic forcing combine to produce and preserve the G1 fan  
 565 sequence. Over the same period, curiously, no terraces are detected in the lower Toro Basin. Three  
 566 possible explanations for this absence (which are not mutually exclusive) include: (1) due to their more  
 567 central position within the basin, the lower reaches of the Río Toro were not strongly affected by rock  
 568 uplift, meaning that any changes in river-channel elevation are not persevered in the geomorphic record  
 569 due to low or a lack of net incision; (2) channels in the lower Toro Basin continued to experience  
 570 aggradation or remained stable at this time, due to feedbacks in the system whereby incision upstream  
 571 caused a pulse of sediment for downstream reaches; or (3) the response time of the Río Toro within the  
 572 lower basin was substantially longer than the forcing period of the aggradation-incision cycles, meaning  
 573 perturbations to the channel-bed elevation due to climate forcing would not have reached so far  
 574 downstream.  
 575



576  
 577 **Fig. 8.** Cartoon illustrating periods of aggradation and incision in the upper and lower Toro Basin from ca. 0.98 Ma (also see  
 578 Table 3). Area of Lower Toro Basin block shaded in grey was not part of this study. A) From 0.98Ma: Base level lowered to  
 579 present day levels, following the deposition of Alfarcito Conglomerates. Renewed hydrological connectivity likely led to  
 580 extensive sediment evacuation and incision of (paleo)topography. Deposition of Quaternary Terrace Conglomerates started  
 581 from 0.94 Ma (Hilley and Strecker, 2005). B) ca. 800-500 ka: G1 fan formation and abandonment during a phase of net incision  
 582 in the upper basin, linked to the MPT. Aggradation was recorded in the lower basin (Tofelde et al., 2017). C) ca. 500-110 ka:  
 583 100-kyr cycles of aggradation and incision recorded by lower basin cut-and-fill terraces (T6 [ca. 490–450 ka], T5 [ca. 370 ka],  
 584 T4 [ca. 285–260 ka], T3 [ca. 170 ka]). No significant geomorphic change recognised in the tributaries of the upper basin. D)  
 585 From ca. 110 ka: G2 fan formation and abandonment in the upper basin, linked to ca. 21/40 kyr climate cycles. Continuation  
 586 of 100-kyr cycles recorded by lower basin terraces (T2 [ca. 110–75 ka], T1 [ $< 75$  ka]).

587  
588

**Table 3.** Summary of upper and lower Toro Basin evolution

UPPER BASIN		LOWER BASIN		
Process/event	Hypotheses <i>(not mutually exclusive)</i>	Process/event	Hypotheses <i>(not mutually exclusive)</i>	
<b>From ca. 0.98 Ma</b> (Fig. 8A)	Base level lower than modern	(i) Renewed hydrological connectivity triggers incision	Base level lower than modern	(i) Renewed hydrological connectivity triggers incision
			Deposition of 'Terrace Conglomerates'	(i) Uplift-induced basin infilling
<b>ca. 800–500 ka</b> (Fig. 8B)	Net incision recorded by G1 fan sequence	(i) Enhanced glacial cycles trigger incision (ii) Uplift of Sierra de Pascha Sur	Stability / continued deposition	(i) Lower reaches minimal affected by uplift
				(ii) System feedbacks promote stability/aggradation (iii) Response time exceeds forcing period
<b>ca. 500–110 ka</b> (Fig. 8C)	No activity recorded	(i) Restricted hydrological connectivity (ii) Downstream incision not yet propagated to upper basin	100-kyr cut-and-fill sedimentary cycles and net incision recorded by fluvial terraces	(i) Eccentricity-driven climate forcing, with continued uplift
<b>From ca. 110 ka</b> (Fig. 8D)	G2 fan aggradation-incision cycles and net incision	(i) Surface abandonment during intensified SASM/glacial periods		base-level drop causing net incision

616  
617  
618  
619  
620  
621  
622  
623  
624  
625  
626  
627  
628  
629

630 To elaborate on the first possibility, the Sierra de Pascha catchments are positioned behind and  
631 perpendicular to west-tilted and deformed basin strata (Barres Sandstone, Agujas and Alfracito  
632 Conglomerates, lava flows) (Fig. 2A). In concert with the work by Hilley and Strecker (2005), we  
633 suggest that channel incision through the resistant sedimentary units accelerated sometime between  
634 0.98 and 0.8 Ma. Once this incision propagated upstream, the removal of weakly consolidated  
635 sedimentary units in the upper basin was likely efficient (Hilley and Strecker, 2005). This evolving  
636 topography could therefore help to explain the net incision needed in the upper Toro Basin to preserve  
637 the alluvial fan surfaces between ca. 800 to 500 ka, and why terrace levels in the lower basin are not  
638 recognised during this time interval.

639

640 To elaborate on the second and third possibilities, as late Quaternary glaciations were limited to the  
641 Pascha tributary headwaters (< 5 km from headwall), the hillslope geomorphic response to prolonged  
642 and intensified glaciation may have been very localized (Tofelde et al., 2018). This is apparently true  
643 for the Iglesia and Calingasta Basins in the Western Precordillera where the tributaries, rather than the  
644 main basin record incision following the Mid-Pleistocene Transition (Terrizzano et al., 2017; Peri et al.,  
645 2022). Following this argument, the response time of the Río Toro's long profile to the 100-kyr climate  
646 cycles after the Mid-Pleistocene Transition (ca. 1.2 to 0.8 Ma) may have been substantially longer than  
647 the period of external forcing. If true, this implies that while upstream reaches of the channel may have  
648 experienced no (or a very low amplitude) aggradation/incision cycles (Allen, 2008; McNab et al., 2023).  
649 Alternatively, feedbacks within the system could lead to differences not only in the magnitude of  
650 aggradation/incision, but also the timing. For example, in southwest Peru, Steffan et al. (2009, 2010),  
651 interpreted aggradation in downstream reaches of river channels during past wet climate periods to  
652 result from pulses of sediment mobilized from hillslopes and upstream channel incision.

653

#### 654 *5.2.2 Terrace formation from ca. 500 to 110 ka*

655 From ca. 500 to 110 ka in the upper Toro Basin, we find no record of fan formation (Fig. 8). Curiously  
656 again, though, the lower Toro Basin exhibits a spectacular sequence of terraces showing 100-kyr  
657 cyclicity starting from ca. 500 ka (Tofelde et al., 2017). If long channel response times explain the lack  
658 of terraces from ca. 800 – 500 ka in the lower Toro Basin, to explain the terraces identified in the lower  
659 basin ca. 500 ka (Tofelde et al., 2017), the channel response time must have changed. This could have  
660 occurred as a result of incision in the upper Toro Basin, which would have narrowed the upstream river  
661 valleys, consequently decreasing river response times and enabling aggradation-incision cycles to affect  
662 channel reaches farther downstream (e.g., McNab et al., 2023).

663

664 While a shortened channel response time can explain the formation of terraces in the lower Toro Basin,  
665 it does not explain the absence of terraces/fans in the upper basin over the same period. Consequently,

666 we next consider other factors that might lead to differences in fan/terrace preservation between the  
667 upper and lower Toro basins.

668

669 Perturbations at the Río Toro outlet, such as a shift in base level, will propagate upstream over time,  
670 thus driving the net incision needed to preserve variations in channel bed elevation in the terrace and  
671 fan sequences. Alternatively, activity along the Gólgota Fault at this time may have adjusted the base  
672 level for the trunk stream. Regardless of the exact trigger for base-level fall (e.g., renewed fluvial  
673 connectivity, possibly enhanced by a drop in Lerma Valley lake level) (Malamud et al., 1996; González  
674 Bonorino and Abascal, 2012), a net incisional wave would have propagated upstream from the lower  
675 basin or outlet. That incision would have facilitated terrace preservation in the lower Toro Basin before  
676 the incisional wave propagated upstream to the upper Toro Basin. Steepened reaches of both the trunk  
677 stream and tributaries up to an elevation of ca. 3400 m (Fig. 2C) are consistent with an upstream  
678 propagating wave of incision, which probably only recently reached the ca. 3300-m elevation of the G2  
679 fan toes.

680

681 Consistent with this interpretation, both the upper and lower Toro basins preserve geomorphic evidence  
682 of channel-bed elevation lowering after ca. 100 ka (terraces T2 and T1 in the lower Toro Basin; G2 fan  
683 generation in the upper Toro Basin). Whereas T2 and T1 lie 40 m and 20 m respectively above the  
684 modern Río Toro, the G2 fans are at most 10 m above their closest channel. This finding further supports  
685 the idea that net incision is ongoing in the lower Toro Basin, probably keeping pace with the ongoing  
686 uplift of the Sierra de Pascha Sur (Tofelde et al., 2017), but net incision has possibly only resumed  
687 within the last ca. 110 to 50 kyr in the upper Toro Basin.

688

689 Other factors may have also played a role in the misaligned timing of fan/terrace formation in the upper  
690 and lower Toro basins. Restricted hydrological connectivity or disconnectivity can lead to internal  
691 variability in the nature and timing of a basin's geomorphic or sedimentary response to external  
692 perturbations (Fryirs et al., 2007; Buter et al., 2022). For example, basin connectivity and geometry  
693 appear to have disrupted the timing of climate-driven sediment transfer within the Humahuaca Basin of  
694 NW Argentina during the last glacial cycles, leading to anti-phased timing of aggradation-incision  
695 cycles along tributaries on either side of the valley (Schildgen et al., 2016). No fault lines, which can  
696 influence connectivity (Guarnieri and Pirrotta, 2008; Brocard et al., 2012), intersect the channel network  
697 between the alluvial fans and terrace levels of the Toro Basin (Fig 2) (Pingel et al., 2020). Nevertheless,  
698 minor adjustments to the long profile of an alluvial channel network can be sufficient to affect the  
699 internal connectivity of a basin (Savi et al., 2020). One such adjustment may include the tributary  
700 junction fan at the Quebrada de Chorro outlet, which has created a diffuse knickzone in the Río Toro  
701 long profile (Fig. 2B). As the fan has aggraded, it has pushed the main channel to the opposite valley  
702 side, evidenced by a marked channel bend. The fan may therefore inhibit the coupling between the



703 upstream and downstream reaches of the trunk stream by disrupting the flow of sediment and (possibly)  
704 water from the Sierra de Pascha tributaries and along the Río Toro (e.g., Harvey 2012). However, the  
705 capacity of the fan to disrupt environmental signals moving through the basin may depend on the  
706 direction of signal travel. For example, channel incision due to a climate-induced increase in water  
707 discharge may continue to propagate downstream, regardless of a new sedimentary input from a major  
708 tributary, unless the tributary fully dams the upstream section. However, if a wave of incision is instead  
709 migrating upstream, a tributary junction fan may slow or disrupt its propagation (Savi et al., 2020).  
710 Nevertheless, while sedimentary inputs from individual tributaries can affect the modern channel  
711 profile, and may slow upstream-propagating incisional cycles, it is not clear whether such localized  
712 features will play an important role in channel network evolution over longer (e.g., > 100 kyr)  
713 timescales.

714

### 715 *5.2.3 Fan formation since ca. 110 ka*

716 All G2 surfaces were either stable or actively receiving sediment for some time during both cool, wet  
717 glacial periods and warm, dry interglacials. Similar to the terraces in the lower basin (Tofelde et al.,  
718 2017), the timing of G2 surface abandonment is restricted to glacial phases; enhanced moisture  
719 availability due to an intensified SASM is likely to have amplified sediment transport and channel  
720 incision (Baker and Fritz, 2015). Around the latitude of the Toro Basin, glacial moraine records in the  
721 Central Andes show strong evidence for glacial advances at ca. 16 and 22–24 ka, with some evidence  
722 also for advances at ca. 42 and e.g. 20/55 ka (D’Arcy et al., 2019a; Fig 7B). The stratigraphically highest  
723 surfaces in G2, Qf\_5 and Qf\_6, show abandonment ages that are consistent with the timing of the oldest  
724 glacial advances recorded in the moraine record (ca. 55 ka).

725

726 For surfaces Qf\_7 and Qf\_8, the timing of abandonment is harder to interpret, due to the difficulty in  
727 knowing whether the youngest boulders on each surface are outliers due to erosion/rotation, or if they  
728 represent a time of active deposition on the surface. Given the similarities in surface weathering between  
729 Qf\_6 and Qf\_7, it is possible that Qf\_7 was active at the same time as Qf\_6 and Qf\_5, and hence was  
730 abandoned at a similar time (implying that the youngest boulder of Qf\_7 is an outlier). If the young  
731 boulder instead represents a real depositional age, then the abandonment of Qf\_7 could be linked to the  
732 ca. 22–24 ka glacial advance, coinciding with the northern hemisphere Last Glacial Maximum. The  
733 abandonment of Qf\_8 is similarly challenging to interpret, with abandonment potentially linked to either  
734 the ca. 24 ka glacial advance (associated with the ‘Minchin’ wet climate phase of the Central Andes) if  
735 the youngest boulder is excluded, or the ca. 16 ka glacial advance associated with Heinrich Stadial 1 if  
736 not excluded.

737

738 While we reason that the two youngest ages from Qf\_7 and Qf\_8 are not outliers and instead reflect  
739 later deposition events (see 5.1.2), we have also estimated the timing of surface abandonment without  
740 them (Fig. 7). In this alternative record, the abandonment of three of the four fans fall between ca. 65  
741 and 60 ka. This points to a modest phase of net incision in several Sierra de Pascha catchments during  
742 a dry interglacial period (Fritz et al., 2007).

743

744 Overall, the exposure age distributions and estimated abandonment ages appear to capture cycles of fan  
745 aggradation-incision with relatively high periodicity. Considering the above tentative links between  
746 abandonment times and glacial advances, and that no known tectonic forcing in the Toro Basin can  
747 explain this cyclicity, the alluvial channel network is likely responding to precession (21-kyr) or  
748 obliquity-driven (40-kyr) climate cycles. Precessional forcing has been recorded within the sedimentary  
749 archives elsewhere in the Central Andes, including fluvial terraces in the Humahuaca Basin (23°S)  
750 (Schildgen et al., 2016) and alluvial fans in the Santa María Basin (26.5°S) (D'Arcy et al., 2018) in NW  
751 Argentina.

752

### 753 **5.3 Impacts of the Mid-Pleistocene Transition on the Toro Basin**

754 The G1 fan surfaces have CRN exposure ages that span several glacial-interglacial cycles (Fig. 6).  
755 Although our interpreted ages are too imprecise to associate with specific glacial phases, 100-kyr glacial  
756 moderation of aggradation-incision cycles is thought to have controlled fluvial terrace formation in the  
757 lower Toro Basin (e.g., Tofelde et al., 2017). In semi-arid landscapes and transport-limited systems, this  
758 finding is not unexpected, as geomorphic activity is invariably amplified during wetter, glacial periods  
759 (Harvey et al., 1999; Spelz et al., 2008; Cesta and Ward, 2016). Given the number of G1 fans (n=4)  
760 capturing the prolonged net incisional phase (>300 kyr), it is possible that eccentricity-driven cycles of  
761 aggradation and incision are also recorded in the upper Toro Basin.

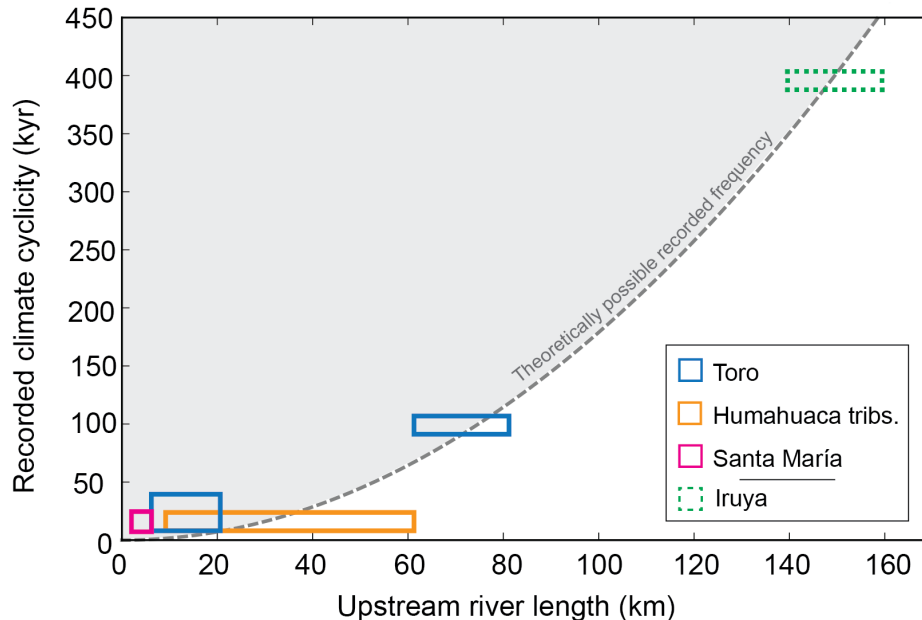
762

763 Our net incisional phase between ca. 800 and 500 ka coincides with the onset of prolonged and enhanced  
764 global glacial cycles following the Mid-Pleistocene Transition (MPT, 1.2–0.8 Ma) which marked a shift  
765 in climate periodicity from 41 to 100 kyr cycles (Berger et al., 1999). The southward migration of the  
766 ITCZ at this time led to heightened moisture availability throughout the Central Andes (Haselton et al.,  
767 2002; Broccoli et al., 2006; Vizy and Cook, 2007). Alluvial channels in semi-arid regions of the Central  
768 Andes are found to respond quickly to marked shifts in precipitation such as this (e.g., Schildgen et al.,  
769 2016; Tofelde et al., 2017), which also appear to drive phases of enhanced sediment evacuation to the  
770 foreland (Fisher et al., 2023).

771

772 Enhanced incision likely linked to the MPT has also been recognised at other locations in the Central  
773 Andes (Fig. 1A), including the Casa Grande Basin (23°S) in the Eastern Cordillera, the Salinas Grandes

774 Basin (23.5°S) of the Puna Plateau (Pingel et al., 2019b), and the Iglesia (30.5°S) and Calingasta (32°S)  
 775 basins in the Western Precordillera (Terrizzano et al., 2017; Peri et al., 2022). These observations point  
 776 to a regional phase of net incision and therefore landscape response to global climate change. For several  
 777 of these locations, including the Toro Basin, local tectonic activity may have provided a secondary  
 778 driver for incision, or created conditions conducive to fan/terrace preservation. Towards the Andean  
 779 interior, the geomorphic response to the MPT probably lessens, as moisture and the extent of past  
 780 glaciations is more restricted (Luna et al., 2018; Haselton et al., 2002). Beyond the Central Andes,  
 781 fluvial terraces along the Río Deseado (47°S) (Tobal et al., 2021) and Río Santa Cruz (50°S) (Milanez  
 782 Fernandes, 2023), draining the Southern Andes in Patagonia also record a period of net incision that  
 783 can be tentatively linked to the MPT. On a global scale, a growing number of studies have identified  
 784 periods of intensified erosion at this time, for example in the St. Elias mountains, Alaska (Gulick et al.,  
 785 2015), Central Appalachia (Del Vecchio et al., 2022), the Rocky Mountains (Pederson and Egholm,  
 786 2013) and the European Alps (Haeuselmann et al., 2007; Valla et al., 2011; Sternai et al., 2013). While  
 787 it is not possible to discount a tectonic influence on landscape change in the upper Toro basin entirely  
 788 due to some chronological ambiguity in the datasets and inherent challenges in deconvolving different  
 789 forcing mechanisms, the links between MPT climate and incision, and its expression elsewhere in the  
 790 Andes and beyond, is compelling.  
 791



792  
 793 **Figure 9.** Correlation between recorded climate cyclicality and upstream river length recognised in four basins of the Central  
 794 Andes: Toro (this study; Tofelde et al., 2017), Humahuaca (Schildgen et al., 2016), Santa María (D’Arcy et al., 2018); Iruya  
 795 (Fisher et al., 2016). Unlike the other records of aggradation and incision, the Iruya record is derived from the basin’s  
 796 sedimentary record and is a paleo-erosion dataset. Adapted from Tofelde et al. (2017). Recorded period:  $0.019 \times \text{river length}^2$ .  
 797

798 **5.4 Climate periodicity and alluvial channel system length**

799 Higher frequency climate cycles are recorded in fan generation G2 of the Sierra de Pascha tributaries  
800 compared with the mainstem of the basin; the alluvial fans, which appear to record climate cycles with  
801 a periodicity of ca. 20 to 40-kyr have an upstream channel length of ~10 km and are positioned ~30 km  
802 upstream of the terrace sequence showing 100-kyr climate cyclicity dated by Tofelde et al. (2017). This  
803 finding substantiates the theory that the response time of alluvial channel systems to perturbations in  
804 climate depends on system length (Paola et al., 1992; Castelltort and Van Den Driessche, 2003; Godard  
805 et al., 2013; McNab et al., 2023). Evidence of this relationship, together with the dependency on the  
806 square of the system length, was identified in the archive of several sedimentary basins in the Central  
807 Andes, although only a single forcing frequency was recorded within each basin (Fig. 9) (Tofelde et al.,  
808 2017). Our new data from the Toro Basin provide critical field evidence that multiple climate  
809 periodicities can be preserved within the sedimentary record of a single sedimentary basin, with higher  
810 forcing frequencies recorded only in the uppermost reaches of the basin.

811

## 812 **6. Conclusions**

813

814 The alluvial fan and terrace sequences of the Toro basin present an excellent opportunity to explore (1)  
815 how channel responses to external perturbations may or may not propagate downstream, and (2) the  
816 differences in landscape response to forcing frequency as a function of stream length. We applied CRN  
817 dating to a suite of alluvial fan surfaces to characterise the evolution of the alluvial channel network of  
818 the Toro basin over the last one million years. Our key findings are as follows:

819

- 820 1. We identified two generations of fan surfaces (G1 and G2) were identified in the Sierra de  
821 Pascha tributary catchments. The G1 fans record CRN exposure ( $^{10}\text{Be}$ ) ages between ca. 800  
822 and 500 ka, whereas the G2 fans record surface activity and then abandonment between ca. 100  
823 and 20 ka.
- 824 2. The G1 fans capture a significant phase of net incision (~ 200 m) between ca. 800 and 500 ka.  
825 The stepwise evacuation of the upper basin coincides with the onset of prolonged and enhanced  
826 global glacial cycles following the Mid-Pleistocene Transition (MPT). With several basins in  
827 the Central Andes and beyond also registering this phase of incision, we propose that the G1  
828 fans are part of a continental scale response to MPT climate change.
- 829 3. The abandonment of the G2 fans is restricted to glacial periods, possibly modulated by 21/40-  
830 kyr climate cycles; enhanced moisture availability due to an intensified SASM likely amplified  
831 channel incision and sediment transport.
- 832 4. Differences in the timing of alluvial fan and fluvial terrace development in the upper and lower  
833 Toro basins appear to be associated with how channel length affects fluvial response time to  
834 climate forcing as well as local controls on net incision, which facilitates preservation of the  
835 geomorphic record of aggradation-incision cycles.

836 5. The new alluvial fan record from the upper Toro Basin, combined with earlier results on fluvial  
837 terraces from the lower Toro Basin, provides field evidence for the theoretical predictions of a  
838 scaling relationship between climate forcing frequency recorded in sedimentary archives and  
839 the system length. We show that multiple climate periodicities can be preserved within the  
840 sedimentary record of a single sedimentary basin, with higher forcing frequencies recorded only  
841 in the uppermost reaches of the basin. This improved understanding of the role of system length  
842 in climate signal propagation is an important step forward in helping us to anticipate the spatial  
843 distribution of sedimentary paleoclimate records within landscapes.

844  
845

#### 846 **7. Code/data availability**

847 All data is included as part of the manuscript.

848

#### 849 **8. Author contribution**

850 Conceptualization: E.N.O, T.F.S, S.T; Sample collection and processing: E.N.O, T.F.S, S.T, H.W.;

851 Visualization: E.N.O with feedback from all authors; Writing & editing: all authors.

852

#### 853 **9. Competing interests**

854 The authors declare that they have no conflict of interest.

855

#### 856 **10. Acknowledgments**

857 This work was co-funded by (1) the German Research Foundation (DFG) grant 373/34-1 and the  
858 Brandenburg Ministry of Sciences, Research, and Cultural Affairs, within the framework of the  
859 International Research Training Group IGK2018 SuRfAce processes, TEctonics and Georesources: The  
860 Andean foreland basin of Argentina (StRATEGy) and (2) the European Research Council (ERC) under  
861 the European Union's Horizon 2020 Research and Innovation program (ERC Consolidator Grant  
862 863490 to T.F.S.). TanDEM-X 12-m resolution digital elevation data were provided by the German  
863 Aerospace Center (DLR) through grant DEM\_GEOL1915 to T.F. S. We thank Yanina Rojo for logistical  
864 support leading up to and during all field work. We also thank Peter van der Beek for assistance during  
865 field work.

866

#### 867 **11. References**

868

869 Alonso, R.N. Estratigrafía del Cenozoico de la cuenca de Pastos Grandes (Puna Salteña) con énfasis  
870 en la Formación. *Revista de la Asociación Geológica Argentina*, 47(2), 189-199.1992.

871 Armitage, J.J., Dunkley Jones, T., Duller, R.A., Whittaker, A.C., Allen, P.A. Temporal buffering of  
872 climate-driven sediment flux cycles by transient catchment response. *Earth and Planetary  
873 Science Letters*, 369–370, 200–210. <https://doi.org/10.1016/j.epsl.2013.03.020>, 2013.

874 Baker, P.A., Rigsby, C.A., Seltzer, G.O., Fritz, S.C., Lowenstein, T.K., Bacher, N.P., Veliz, C. Tropical  
875 climate changes at millennial and orbital timescales on the Bolivian Altiplano. *Nature*,  
876 409(6821), 698-701. <https://doi.org/10.1038/35055524>, 2001.

877 Baker, P.A., Fritz, S.C. Nature and causes of Quaternary climate variation of tropical South America.  
878 *Quaternary Science Reviews.*, 124, 31-47. <https://doi.org/10.1016/j.quascirev.2015.06.011>,  
879 2015.

880 Berger, A., Li, X.S., Loutre, M.F. Modelling northern hemisphere ice volume over the last 3 Ma.  
881 *Quaternary Science Reviews*, 18(1), 1-11. [https://doi.org/10.1016/S0277-3791\(98\)00033-X](https://doi.org/10.1016/S0277-3791(98)00033-X),  
882 1999.

883 Berger, A., Loutre, M.F. Insolation values for the climate of the last 10 million years. *Quaternary  
884 Science Reviews*, 10(4), 297-317. [https://doi.org/10.1016/0277-3791\(91\)90033-Q](https://doi.org/10.1016/0277-3791(91)90033-Q), 1991.

- 885 Bernard, T., Sinclair, H.D., Gailleton, B., Mudd, S.M., Ford, M. Lithological control on the post-  
886 orogenic topography and erosion history of the Pyrenees. *Earth and Planetary Science Letters*,  
887 518, 53–66. <https://doi.org/10.1016/j.epsl.2019.04.034>, 2019.
- 888 Blard, P.-H., Braucher, R., Lavé, J., Bourlès, D. Cosmogenic  $^{10}\text{Be}$  production rate calibrated against  
889  $^3\text{He}$  in the high Tropical Andes (3800–4900 m, 20–22° S). *Earth and Planetary Science Letters*,  
890 382, 140–149. <https://doi.org/10.1016/j.epsl.2013.09.010>, 2013.
- 891 Bobst, A.L., Lowenstein, T.K., Jordan, T.E., Godfrey, L.V., Ku, T.L., Luo, S. A 106 ka paleoclimate  
892 record from drill core of the Salar de Atacama, northern Chile. *Palaeogeography,*  
893 *Palaeoclimatology, Palaeoecology*, 173(1-2), 21–42. [https://doi.org/10.1016/S0031-](https://doi.org/10.1016/S0031-0182(01)00308-X)  
894 [0182\(01\)00308-X](https://doi.org/10.1016/S0031-0182(01)00308-X), 2001.
- 895 Bonorino, G.G., Abascal, L. Drainage and base-level adjustments during evolution of a late Pleistocene  
896 piggyback basin, Eastern Cordillera, Central Andes of northwestern Argentina. *Bulletin*,  
897 124(11-12), 1858–1870. <https://doi.org/10.1130/B30395.1>, 2012.
- 898 Bookhagen, B., Strecker, M.R. Orographic barriers, high-resolution TRMM rainfall, and relief  
899 variations along the eastern Andes. *Geophysical Research Letters*, 35.  
900 <https://doi.org/10.1029/2007GL032011>, 2008.
- 901 Bridgland, D., Westaway, R. Climatically controlled river terrace staircases: a worldwide Quaternary  
902 phenomenon. *Geomorphology*, 98(3-4), 285–315,  
903 <https://doi.org/10.1016/j.geomorph.2006.12.032>, 2008.
- 904 Brocard, G., Willenbring, J., Suski, B., Audra, P., Authemayou, C., Cosenza-Murales, B., Morán-Ical,  
905 S., Demory, F., Rochette, P., Vennemann, T., Holliger, K. Rate and processes of river network  
906 rearrangement during incipient faulting: The case of the Cahabón River, Guatemala. *American*  
907 *Journal of Science*, 312(5), 449–507, <https://doi.org/10.2475/05.2012.01>, 2012.
- 908 Broccoli, A.J., Dahl, K.A., Stouffer, R.J. Response of the ITCZ to Northern Hemisphere cooling.  
909 *Geophysical Research Letters*, 33(1). <https://doi.org/10.1029/2005GL024546>, 2006.
- 910 Brooke, S.A., Whittaker, A.C., Armitage, J.J., D'Arcy, M., Watkins, S.E. Quantifying sediment  
911 transport dynamics on alluvial fans from spatial and temporal changes in grain size, Death  
912 Valley, California. *Journal of Geophysical Research: Earth Surface*, 123(8), 2039–2067.  
913 <https://doi.org/10.1029/2018JF004622>, 2018.
- 914 Bufe, A., Burbank, D.W., Liu, L., Bookhagen, B., Qin, J., Chen, J., Li, T., Thompson Jobe, J.A., Yang,  
915 H. Variations of lateral bedrock erosion rates control planation of uplifting folds in the foreland  
916 of the Tian Shan, NW China. *Journal of Geophysical Research: Earth Surface*, 122(12), 2431–  
917 2467. <https://doi.org/10.1002/2016JF004099>, 2017.
- 918 Buter, A., Heckmann, T., Filisetti, L., Savi, S., Mao, L., Gems, B., Comiti, F. Effects of catchment  
919 characteristics and hydro-meteorological scenarios on sediment connectivity in glacierised  
920 catchments. *Geomorphology*, 402, 108128. <https://doi.org/10.1016/j.geomorph.2022.108128>,  
921 2022.
- 922 Castelltort, S., Van Den Driessche, J. How plausible are high-frequency sediment supply-driven cycles  
923 in the stratigraphic record? *Sedimentary Geology*, 157, 3–13. [https://doi.org/10.1016/S0037-](https://doi.org/10.1016/S0037-0738(03)00066-6)  
924 [0738\(03\)00066-6](https://doi.org/10.1016/S0037-0738(03)00066-6), 2003.
- 925 Castino, F., Bookhagen, B., Strecker, M.R. Rainfall variability and trends of the past six decades (1950–  
926 2014) in the subtropical NW Argentine Andes. *Climate Dynamics*, 48, 1049–1067.  
927 <https://doi.org/10.1007/s00382-016-3127-2>, 2017.
- 928 Cesta, J.M., Ward, D.J. Timing and nature of alluvial fan development along the Chajnantor Plateau,  
929 northern Chile. *Geomorphology*, 273, 412–427.  
930 <https://doi.org/10.1016/j.geomorph.2016.09.003>, 2016.
- 931 Clarke, L., Quine, T.A., Nicholas, A. An experimental investigation of autogenic behaviour during  
932 alluvial fan evolution. *Geomorphology*, 115(3-4), 278–285.  
933 <https://doi.org/10.1016/j.geomorph.2009.06.033>, 2010.
- 934 Counts, R.C., Murari, M.K., Owen, L.A., Mahan, S.A., Greenan, M. Late Quaternary  
935 chronostratigraphic framework of terraces and alluvium along the lower Ohio River,  
936 southwestern Indiana and western Kentucky, USA. *Quaternary Science Reviews*, 110, 72–91.  
937 <https://doi.org/10.1016/j.quascirev.2014.11.011>, 2015.
- 938 Crivellari, S., Chiessi, C.M., Kuhnert, H., Häggi, C., da Costa Portilho-Ramos, R., Zeng, J.Y., Zhang,  
939 Y., Schefuß, E., Mollenhauer, G., Hefter, J., Alexandre, F. Increased Amazon freshwater

940 discharge during late Heinrich Stadial 1. *Quaternary Science Reviews*, 181, 144-155.  
941 <https://doi.org/10.1016/j.quascirev.2017.12.005>, 2018.

942 D'Arcy, M.K., Schildgen, T.F., Strecker, M.R., Wittmann, H., Duesing, W., Mey, J., Tofelde, S.,  
943 Weissmann, P., Alonso, R.N. Timing of past glaciation at the Sierra de Aconquija, northwestern  
944 Argentina, and throughout the Central Andes. *Quaternary Science Reviews*, 204, 37–57.  
945 <https://doi.org/10.1016/j.quascirev.2018.11.022>, 2019a.

946 D'Arcy, M.K., Schildgen, T.F., Turowski, J.M., Dinezio, P. Inferring the timing of abandonment of  
947 aggraded alluvial surfaces dated with cosmogenic nuclides. *Earth Surface Dynamics*, 7, 755–  
948 771. <https://doi.org/10.5194/esurf-7-755-2019>, 2019b.

949 D'Arcy, M., Schildgen, T.F., Tofelde, S., Strecker, M.R., Wittmann, H., Düsing, W., Weissmann, P.  
950 and Roda-Boluda, D.C. Catchment-alluvial fan systems record > 200 ka of millennial-scale  
951 climate changes in the subtropical Andes. EGU General Assembly Conference Abstracts.  
952 <https://ui.adsabs.harvard.edu/abs/2018EGUGA..20.4710D/abstract>, 2018.

953 DeCelles, P.G., Carrapa, B., Horton, B.K., Gehrels, G.E. Cenozoic foreland basin system in the central  
954 Andes of northwestern Argentina: Implications for Andean geodynamics and modes of  
955 deformation. *Tectonics*, 30(6). <https://doi.org/10.1029/2011TC002948>, 2011.

956 Del Vecchio, J., DiBiase, R.A., Corbett, L.B., Bierman, P.R., Caffee, M.W., Ivory, S.J. Increased  
957 erosion rates following the onset of Pleistocene periglaciation at Bear Meadows, Pennsylvania,  
958 USA. *Geophysical Research Letters*, 49(4), p.e2021GL096739.  
959 <https://doi.org/10.1029/2021GL096739>, 2022.

960 Dey, S., Thiede, R.C., Schildgen, T.F., Wittmann, H., Bookhagen, B., Scherler, D., Jain, V., Strecker,  
961 M.R. Climate-driven sediment aggradation and incision since the late Pleistocene in the NW  
962 Himalaya, India. *Earth and Planetary Science Letters*, 449, 321–331.  
963 <https://doi.org/10.1016/j.epsl.2016.05.050>, 2016.

964 Dortch, J.M., Tomkins, M.D., Saha, S., Murari, M.K., Schoenbohm, L.M., Curl, D. A tool for the ages:  
965 The Probabilistic Cosmogenic Age Analysis Tool (P-CAAT). *Quaternary Geochronology*, 71,  
966 101323. <https://doi.org/10.1016/j.quageo.2022.101323>, 2022.

967 Dühnforth, M., Densmore, A.L., Ivy-Ochs, S., Allen, P., Kubik, P.W. Early to Late Pleistocene history  
968 of debris-flow fan evolution in western Death Valley (California) using cosmogenic <sup>10</sup>Be and  
969 <sup>26</sup>Al. *Geomorphology*, 281, 53–65. <https://doi.org/10.1016/j.geomorph.2016.12.020>, 2017.

970 Dühnforth, M., Densmore, A.L., Ivy-Ochs, S., Allen, P.A., Kubik, P.W. Timing and patterns of debris  
971 flow deposition on Shepherd and Symmes creek fans, Owens Valley, California, deduced from  
972 cosmogenic <sup>10</sup>Be. *Journal of Geophysical Research: Earth Surface*, 112.  
973 <https://doi.org/10.1029/2006JF000562>, 2007.

974 Dunai, T.J., López, G.A.G., Juez-Larré, J. Oligocene–Miocene age of aridity in the Atacama Desert  
975 revealed by exposure dating of erosion-sensitive landforms. *Geology*, 33(4), 321-324.  
976 <https://doi.org/10.1130/G21184.1>, 2005.

977 Fernandes, V.M., Schildgen, T., Ruby, A., Wittmann-Oelze, H., McNab, F. Pleistocene Landscape  
978 Evolution in Southern Patagonia: A Record of Regional Incision from <sup>10</sup>Be Dating of Fluvial  
979 Terraces (No. EGU23-15938). Copernicus Meetings. <https://doi.org/10.5194/egusphere-egu23-15938>, 2023.

981 Fisher, G.B., Luna, L.V., Amidon, W.H., Burbank, D.W., de Boer, B., Stap, L.B., Bookhagen, B.,  
982 Godard, V., Oskin, M.E., Alonso, R.N., and Tuenter, E. Milankovitch-paced erosion in the  
983 southern Central Andes. *Nature Communications*, 14(1), 424 <https://doi.org/10.1038/s41467-023-36022-0>, 2023.

985 Fritz, S.C., Baker, P.A., Ekdahl, E., Seltzer, G.O., Stevens, L.R. Millennial-scale climate variability  
986 during the Last Glacial period in the tropical Andes. *Quaternary Science Reviews*, 29(7-8),  
987 1017-1024. <https://doi.org/10.1016/j.quascirev.2010.01.001>, 2010.

988 Fritz, S.C., Baker, P.A., Seltzer, G.O., Ballantyne, A., Tapia, P., Cheng, H., Edwards, R.L. Quaternary  
989 glaciation and hydrologic variation in the South American tropics as reconstructed from the  
990 Lake Titicaca drilling project. *Quaternary Research*, 68(3), 410-420.  
991 <https://doi.org/10.1016/j.yqres.2007.07.008>, 2007.

992 Fritz, S.C., Baker, P.A., Lowenstein, T.K., Seltzer, G.O., Rigsby, C.A., Dwyer, G.S., Tapia, P.M.,  
993 Arnold, K.K., Ku, T.L., Luo, S. Hydrologic variation during the last 170,000 years in the

- 994 southern hemisphere tropics of South America. *Quaternary Research*, 61(1), 95-104.  
 995 <https://doi.org/10.1016/j.yqres.2003.08.007>, 2004.
- 996 Fryirs, K.A., Brierley, G.J., Preston, N.J., Kasai, M. Buffers, barriers and blankets: The (dis)  
 997 connectivity of catchment-scale sediment cascades. *Catena*, 70(1), 49-67.  
 998 <https://doi.org/10.1016/j.catena.2006.07.007>, 2007.
- 999 Ganey, P.N., Dolan, J.F., Frankel, K.L., Finkel, R.C. Rates of extension along the Fish Lake Valley  
 1000 fault and transtensional deformation in the Eastern California shear zone–Walker Lane belt.  
 1001 *Lithosphere*, 2(1), 33-49. <https://doi.org/10.1130/L51.1>, 2010.
- 1002 García, V.H., Hongn, F., Cristallini, E.O. Late Miocene to recent morphotectonic evolution and  
 1003 potential seismic hazard of the northern Lerma valley: clues from Lomas de Medeiros,  
 1004 Cordillera Oriental, NW Argentina. *Tectonophysics*, 608, 1238-1253.  
 1005 <https://doi.org/10.1016/j.tecto.2013.06.021>, 2013.
- 1006 Godard, V., Tucker, G.E., Burch Fisher, G., Burbank, D.W., Bookhagen, B. Frequency-dependent  
 1007 landscape response to climatic forcing. *Geophysical Research Letters*, 40, 859–863.  
 1008 <https://doi.org/10.1002/grl.50253>, 2013.
- 1009 Godfrey, L.V., Jordan, T.E., Lowenstein, T.K., Alonso, R.L. Stable isotope constraints on the transport  
 1010 of water to the Andes between 22 and 26 S during the last glacial cycle. *Palaeogeography,*  
 1011 *Palaeoclimatology, Palaeoecology*, 194(1-3), 299-317. [https://doi.org/10.1016/S0031-](https://doi.org/10.1016/S0031-0182(03)00283-9)  
 1012 [0182\(03\)00283-9](https://doi.org/10.1016/S0031-0182(03)00283-9), 2003.
- 1013 Gosling, W.D., Bush, M.B., Hanselman, J.A., Chepstow-Lusty, A. Glacial-interglacial changes in  
 1014 moisture balance and the impact on vegetation in the southern hemisphere tropical Andes  
 1015 (Bolivia/Peru). *Palaeogeography, Palaeoclimatology, Palaeoecology*, 259(1), 35-50.  
 1016 <https://doi.org/10.1016/j.palaeo.2007.02.050>, 2008.
- 1017 Gray, H.J., Owen, L.A., Dietsch, C., Beck, R.A., Caffee, M.A., Finkel, R.C., Mahan, S.A. Quaternary  
 1018 landscape development, alluvial fan chronology and erosion of the Mecca Hills at the southern  
 1019 end of the San Andreas fault zone. *Quaternary Science Reviews*, 105, 66-85.  
 1020 <https://doi.org/10.1016/j.quascirev.2014.09.009>, 2014.
- 1021 Guarnieri, P., Pirrotta, C. The response of drainage basins to the late Quaternary tectonics in the Sicilian  
 1022 side of the Messina Strait (NE Sicily). *Geomorphology*, 95(3-4), 260-273.  
 1023 <https://doi.org/10.1016/j.geomorph.2007.06.013>, 2008.
- 1024 Gulick, S.P., Jaeger, J.M., Mix, A.C., Asahi, H., Bahlburg, H., Belanger, C.L., Berbel, G.B., Childress,  
 1025 L., Cowan, E., Drab, L., Forwick, M. Mid-Pleistocene climate transition drives net mass loss  
 1026 from rapidly uplifting St. Elias Mountains, Alaska. *Proceedings of the National Academy of*  
 1027 *Sciences*, 112(49), 15042-15047. <https://doi.org/10.1073/pnas.1512549112>, 2015.
- 1028 Haeuselmann, P., Granger, D.E., Jeannin, P.Y., Lauritzen, S.E. Abrupt glacial valley incision at 0.8 Ma  
 1029 dated from cave deposits in Switzerland. *Geology*, 35(2), 143-146.  
 1030 <https://doi.org/10.1130/G23094A>, 2007.
- 1031 Hain, M.P., Strecker, M.R., Bookhagen, B., Alonso, R.N., Pingel, H., Schmitt, A.K. Neogene to  
 1032 Quaternary broken foreland formation and sedimentation dynamics in the Andes of NW  
 1033 Argentina (25 S). *Tectonics*, 30(2). <https://doi.org/10.1029/2010TC002703>, 2011.
- 1034 Harvey, A.M. The coupling status of alluvial fans and debris cones: a review and synthesis. *Earth*  
 1035 *Surface Processes and Landforms*, 37(1), 64-76. <https://doi.org/10.1002/esp.2213>, 2012.
- 1036 Harvey, A.M., Silva, P.G., Mather, A.E., Goy, J.L., Stokes, M., Zazo, C. The impact of Quaternary sea-  
 1037 level and climatic change on coastal alluvial fans in the Cabo de Gata ranges, southeast Spain.  
 1038 *Geomorphology*, 28(1-2), 1-22 [https://doi.org/10.1016/S0169-555X\(98\)00100-7](https://doi.org/10.1016/S0169-555X(98)00100-7), 1999.
- 1039 Haselton, K., Hilley, G., Strecker, M.R. Average Pleistocene climatic patterns in the southern central  
 1040 Andes: Controls on mountain glaciation and paleoclimate implications. *The Journal of*  
 1041 *Geology*, 110(2), 211-226. 2002.
- 1042 Hedrick, K., Owen, L.A., Rockwell, T.K., Meigs, A., Costa, C., Caffee, M.W., Masana, E., Ahumada,  
 1043 E. Timing and nature of alluvial fan and strath terrace formation in the Eastern Precordillera of  
 1044 Argentina. *Quaternary Science Reviews*, 80, 143–168  
 1045 <https://doi.org/10.1016/j.quascirev.2013.05.004>, 2013.
- 1046 Hidy, A.J., Gosse, J.C., Pederson, J.L., Mattern, J.P., Finkel, R.C. A geologically constrained Monte  
 1047 Carlo approach to modeling exposure ages from profiles of cosmogenic nuclides: An example



1048 from Lees Ferry, Arizona. *Geochemistry Geophysics Geosystems*, 11, Q0AA10.  
1049 <https://doi.org/10.1029/2010GC003084>, 2010.

1050 Hilley, G.E., Strecker, M.R. Processes of oscillatory basin filling and excavation in a tectonically active  
1051 orogen: Quebrada del Toro Basin, NW Argentina. *Bulletin of the Geological Society of*  
1052 *America*, 117, 887–901. <https://doi.org/10.1130/B25602.1>, 2005.

1053 Howard, A.D. Equilibrium and time scales in geomorphology: Application to sand-bed alluvial streams.  
1054 *Earth Surface Processes and Landforms*, 7(4), pp.303-325.  
1055 <https://doi.org/10.1002/esp.3290070403>, 1982.

1056 Hughes, P.D. Geomorphology and Quaternary stratigraphy: The roles of morpho-, litho-, and  
1057 allostratigraphy. *Geomorphology*, 123, 189–199.  
1058 <https://doi.org/10.1016/j.geomorph.2010.07.025>, 2010.

1059 Imbrie, John., McIntyre, Andrew. SST vs time for core V25-21 (specmap.059). PANGAEA., 2006.

1060 Kelly, M.A., Lowell, T. V., Applegate, P.J., Phillips, F.M., Schaefer, J.M., Smith, C.A., Kim, H.,  
1061 Leonard, K.C., Hudson, A.M. A locally calibrated, late glacial <sup>10</sup>Be production rate from a low-  
1062 latitude, high-altitude site in the Peruvian Andes. *Quaternary Geochronology*, 26, 70–85.  
1063 <https://doi.org/10.1016/j.quageo.2013.10.007>, 2015.

1064 Kleinert, K., Strecker, M.R. Climate change in response to orographic barrier uplift: Paleosol and stable  
1065 isotope evidence from the late Neogene Santa Maria basin, northwestern Argentina. *Geological*  
1066 *Society of America Bulletin*, 113(6), 728-742. [https://doi.org/10.1130/0016-7606\(2001\)113<0728:CCIRTO>2.0.CO;2](https://doi.org/10.1130/0016-7606(2001)113<0728:CCIRTO>2.0.CO;2), 2001.

1068 Kober, F., Zeilinger, G., Ivy-Ochs, S., Dolati, A., Smit, J., Kubik, P.W. Climatic and tectonic control  
1069 on fluvial and alluvial fan sequence formation in the Central Makran Range, SE-Iran. *Global*  
1070 *and Planetary Change*, 111, 133-149. <https://doi.org/10.1016/j.gloplacha.2013.09.003>, 2013.

1071 Lal, D. Cosmic ray labeling of erosion surfaces: in situ nuclide production rates and erosion models.  
1072 *Earth and Planetary Science Letters*, 104, 424–439. [https://doi.org/10.1016/0012-821X\(91\)90220-C](https://doi.org/10.1016/0012-821X(91)90220-C), 1991.

1074 Lifton, N., Sato, T., Dunai, T.J. Scaling in situ cosmogenic nuclide production rates using analytical  
1075 approximations to atmospheric cosmic-ray fluxes. *Earth and Planetary Science Letters*, 386,  
1076 149–160. <https://doi.org/10.1016/j.epsl.2013.10.052>, 2014.

1077 Lisiecki, L.E., Raymo, M.E. Diachronous benthic  $\delta^{18}\text{O}$  responses during late Pleistocene terminations.  
1078 *Paleoceanography*, 24(3). <https://doi.org/10.1029/2009PA001732>, 2009.

1079 Luna, L. V., Bookhagen, B., Niedermann, S., Rugel, G., Scharf, A., Merchel, S. Glacial chronology and  
1080 production rate cross-calibration of five cosmogenic nuclide and mineral systems from the  
1081 southern Central Andean Plateau. *Earth and Planetary Science Letters*, 500, 242–253.  
1082 <https://doi.org/10.1016/j.epsl.2018.07.034>, 2018.

1083 Ma, Y., Stuart, F.M. The use of in-situ cosmogenic <sup>21</sup>Ne in studies on long-term landscape development.  
1084 *Acta Geochimica*, 37, 310-322. <https://doi.org/10.1007/s11631-017-0216-9>, 2018.

1085 Mackin, J. Concept of the graded river. *Geological Society of America Bulletin*, 59(5), 463-512, 1948.

1086 Malamud, B.D., Jordan, T.E., Alonso, R.A., Gallardo, E.F., Gonzalez, R.E., Kelley, S.A. Pleistocene  
1087 Lake Lerma, Salta Province, NW Argentina. In XIII Congreso Geológico Argentino y III  
1088 Congreso de Exploración de Hidrocarburos, Vol. 1, 103-114, 1996.

1089 Marrett, R., Strecker, M.R. Response of intracontinental deformation in the central Andes to late  
1090 Cenozoic reorganization of South American Plate motions. *Tectonics*, 19(3), 452-467.  
1091 <https://doi.org/10.1029/1999TC001102>, 2000.

1092 Marrett, R.A., Allmendinger, R.W., Alonso, R.N., Drake, R.E. Late Cenozoic tectonic evolution of the  
1093 Puna Plateau and adjacent foreland, northwestern Argentine Andes. *Journal of South American*  
1094 *Earth Sciences*, 7(2), 179-207. [https://doi.org/10.1016/0895-9811\(94\)90007-8](https://doi.org/10.1016/0895-9811(94)90007-8), 1994.

1095 Martin, L.C.P., Blard, P.-H., Balco, G., Lavé, J., Delunel, R., Lifton, N., Laurent, V. The CREp program  
1096 and the ICE-D production rate calibration database: A fully parameterizable and updated online  
1097 tool to compute cosmic-ray exposure ages. *Quaternary Geochronology*, 38, 25–49.  
1098 <https://doi.org/10.1016/j.quageo.2016.11.006>, 2017.

1099 Martin, L.C.P., Blard, P.-H., Lavé, J., Braucher, R., Lupker, M., Condom, T., Charreau, J., Mariotti, V.,  
1100 ASTER Team, Davy, E. In situ cosmogenic <sup>10</sup>Be production rate in the High Tropical Andes.  
1101 *Quaternary Geochronology*, 30, 54–68. <https://doi.org/10.1016/j.quageo.2015.06.012>, 2015.

- 1102 Martin, L.C., Blard, P.H., Lavé, J., Condom, T., Prémaillon, M., Jomelli, V., Brunstein, D., Lupker, M.,  
 1103 Charreau, J., Mariotti, V., Tibari, B. Lake Tauca highstand (Heinrich Stadial 1a) driven by a  
 1104 southward shift of the Bolivian High. *Science Advances*, 4(8),  
 1105 <https://doi.org/10.1126/sciadv.aar2514>, 2018.
- 1106 Martini, M.A., Kaplan, M.R., Strelin, J.A., Astini, R.A., Schaefer, J.M., Caffee, M.W., Schwartz, R.  
 1107 Late Pleistocene glacial fluctuations in Cordillera oriental, subtropical Andes. *Quaternary*  
 1108 *Science Reviews*, 171, 245-259. <https://doi.org/10.1016/j.quascirev.2017.06.033>, 2017.
- 1109 Mather, A.E., Stokes, M., Whitfield, E. River terraces and alluvial fans: The case for an integrated  
 1110 Quaternary fluvial archive. *Quaternary Science Reviews* 166, 74-90,  
 1111 <https://doi.org/10.1016/j.quascirev.2016.09.022>, 2017.
- 1112 Mazzuoli, R., Vezzoli, L., Omarini, R., Acocella, V., Gioncada, A., Matteini, M., Dini, A., Guillou, H.,  
 1113 Hauser, N., Uttini, A., Scaillet, S. Miocene magmatism and tectonics of the easternmost sector  
 1114 of the Calama–Olacapato–El Toro fault system in Central Andes at ~ 24 S: Insights into the  
 1115 evolution of the Eastern Cordillera. *GSA Bulletin* 120(11-12), 1493-1517,  
 1116 <https://doi.org/10.1130/B26109.1>, 2008.
- 1117 McFadden, L.D., Ritter, J.B., Wells, S.G. Use of Multiparameter Relative-Age Methods for Age  
 1118 Estimation and Correlation of Alluvial Fan Surfaces on a Desert Piedmont, Eastern Mojave  
 1119 Desert, California. *Quaternary Research* 32, 276–290, [https://doi.org/10.1016/0033-](https://doi.org/10.1016/0033-5894(89)90094-X)  
 1120 [5894\(89\)90094-X](https://doi.org/10.1016/0033-5894(89)90094-X), 1989.
- 1121 McNab, F., Schildgen, T.F., Turowski, J.M., Wickert, A.D. Diverse responses of alluvial rivers to  
 1122 periodic environmental change. *Geophysical Research Letters* 50(10), e2023GL103075,  
 1123 <https://doi.org/10.1029/2023GL103075>, 2023.
- 1124 Mescolotti, P.C., do Nascimento Pupim, F., Ladeira, F.S.B., Sawakuchi, A.O., Santa Catharina, A.,  
 1125 Assine, M.L. Fluvial aggradation and incision in the Brazilian tropical semi-arid: Climate-  
 1126 controlled landscape evolution of the São Francisco River. *Quaternary Science Reviews* 263,  
 1127 106977, <https://doi.org/10.1016/j.quascirev.2021.106977>, 2021.
- 1128 Messenger, G., Huyghe, D., Bonnel, C., Nivière, B., Fasentieux, B. The Neogene to Quaternary evolution  
 1129 of the Neuquén Andes broken foreland forced by tectonic, climatic and surface processes  
 1130 (southern Central Andes). *Journal of South American Earth Sciences*, 131, 104620,  
 1131 <https://doi.org/10.1016/j.jsames.2023.104620>.
- 1132 Mey, J., D'Arcy, M.K., Schildgen, T.F., Egholm, D.L., Wittmann, H., Strecker, M.R. Temperature and  
 1133 precipitation in the southern Central Andes during the last glacial maximum, Heinrich Stadial  
 1134 1, and the Younger Dryas. *Quaternary Science Reviews* 248, 106592,  
 1135 <https://doi.org/10.1016/j.quascirev.2020.106592>, 2020.
- 1136 Mosblech, N.A., Bush, M.B., Gosling, W.D., Hodell, D., Thomas, L., Van Calsteren, P., Correa-Metrio,  
 1137 A., Valencia, B.G., Curtis, J., Van Woesik, R. North Atlantic forcing of Amazonian  
 1138 precipitation during the last ice age. *Nature Geoscience* 5(11), 817-820,  
 1139 <https://doi.org/10.1038/ngeo1588>, 2012.
- 1140 Mouchéné, M., van der Beek, P., Carretier, S., Mouthereau, F. Autogenic versus allogenic controls on  
 1141 the evolution of a coupled fluvial megafan–mountainous catchment system: numerical  
 1142 modelling and comparison with the Lannemezan megafan system (northern Pyrenees, France).  
 1143 *Earth Surface Dynamics* 5(1), 125-143, <https://doi.org/10.5194/esurf-5-125-2017>, 2017.
- 1144 Mouslopoulou, V., Begg, J., Fülling, A., Moraetis, D., Partsinevelos, P., Oncken, O. Distinct phases of  
 1145 eustatic and tectonic forcing for late Quaternary landscape evolution in southwest Crete,  
 1146 Greece. *Earth Surface Dynamics* 5(3), 511-527, <https://doi.org/10.5194/esurf-5-511-2017>,  
 1147 2017.
- 1148 Nicholas, A.P., Quine, T.A. Modeling alluvial landform change in the absence of external  
 1149 environmental forcing. *Geology* 35(6), 527-530, <https://doi.org/10.1130/G23377A.1>, 2007.
- 1150 Nishiizumi, K., Winterer, E.L., Kohl, C.P., Klein, J., Middleton, R., Lal, D., Arnold, J.R. Cosmic ray  
 1151 production rates of <sup>10</sup>Be and <sup>26</sup>Al in quartz from glacially polished rocks. *Journal of Geophysical*  
 1152 *Research* 94, 17907, <https://doi.org/10.1029/JB094iB12p17907>, 1989.
- 1153 Novello, V.F., Cruz, F.W., Vuille, M., Strikis, N.M., Edwards, R.L., Cheng, H., Emerick, S., De Paula,  
 1154 M.S., Li, X., Barreto, E.D.S., Karmann, I. A high-resolution history of the South American  
 1155 Monsoon from Last Glacial Maximum to the Holocene. *Scientific Reports* 7(1), 44267,  
 1156 <https://doi.org/10.1038/srep44267>, 2017.

1157 Orr, E.N., Owen, L.A., Saha, S., Caffee, M.W. Climate-driven late Quaternary fan surface abandonment  
1158 in the NW Himalaya. In: *Untangling the Quaternary Period—A Legacy of Stephen C. Porter*.  
1159 Geological Society of America, 63–80. [https://doi.org/10.1130/2020.2548\(04\)](https://doi.org/10.1130/2020.2548(04)), 2021.

1160 Owen, L.A., Clemmens, S.J., Finkel, R.C., Gray, H. Late Quaternary alluvial fans at the eastern end of  
1161 the San Bernardino Mountains, Southern California. *Quaternary Science Reviews*, 87, 114-  
1162 134. <https://doi.org/10.1016/j.quascirev.2014.01.003>, 2014.

1163 Paola, C., Heller, P.L., Angevine, C.L. The large-scale dynamics of grain-size variation in alluvial  
1164 basins, 1: theory. *Basin Research*. 4, 73-90. [https://doi.org/10.1111/j.1365-  
1165 2117.1992.tb00145.x](https://doi.org/10.1111/j.1365-2117.1992.tb00145.x), 1992.

1166 Pearson, D.M., Kapp, P., DeCelles, P.G., Reiners, P.W., Gehrels, G.E., Ducea, M.N., Pullen, A.  
1167 Influence of pre-Andean crustal structure on Cenozoic thrust belt kinematics and shortening  
1168 magnitude: Northwestern Argentina. *Geosphere*, 9(6), 1766-1782. 2013.  
1169 <https://doi.org/10.1130/GES00923.1>

1170 Pedersen, V.K., Egholm, D.L. Glaciations in response to climate variations preconditioned by evolving  
1171 topography. *Nature*, 493(7431), 206-210. <https://doi.org/10.1038/nature11786>, 2013.

1172 Peri, V.G., Haghpor, N., Christl, M., Terrizzano, C., Kaveh-Firouz, A., Leiva, M.F., Pérez, P., Yamin,  
1173 M., Barcelona, H., Burg, J.P. Quaternary landscape evolution in the Western Argentine  
1174 Precordillera constrained by <sup>10</sup>Be cosmogenic dating. *Geomorphology* 396.  
1175 <https://doi.org/10.1016/j.geomorph.2021.107984>, 2022.

1176 Perron, J.T., Royden, L. An integral approach to bedrock river profile analysis. *Earth Surface Processes  
1177 and Landforms*, 38(6), 570-576. <https://doi.org/10.1002/esp.3302>, 2013.

1178 Pingel, H., Strecker, M.R., Mulch, A., Alonso, R.N., Cottle, J., Rohrmann, A. Late Cenozoic  
1179 topographic evolution of the Eastern Cordillera and Puna Plateau margin in the southern Central  
1180 Andes (NW Argentina). *Earth and Planetary Science Letters* 535, 116112.  
1181 <https://doi.org/10.1016/j.epsl.2020.116112>, 2020.

1182 Pingel, H., Alonso, R.N., Altenberger, U., Cottle, J., Strecker, M.R. Miocene to Quaternary basin  
1183 evolution at the southeastern Andean Plateau (Puna) margin (ca. 24°S lat, Northwestern  
1184 Argentina). *Basin Research* 31, 808–826. <https://doi.org/10.1111/bre.12346>, 2019a.

1185 Pingel, H., Schildgen, T., Strecker, M.R., Wittmann, H. Pliocene–Pleistocene orographic control on  
1186 denudation in northwest Argentina. *Geology* 47, 359–362. <https://doi.org/10.1130/G45800.1>,  
1187 2019b.

1188 Pingel, H., Mulch, A., Alonso, R.N., Cottle, J., Hynek, S.A., Poletti, J., Rohrmann, A., Schmitt, A.K.,  
1189 Stockli, D.F. and Strecker, M.R. Surface uplift and convective rainfall along the southern  
1190 Central Andes (Angastaco Basin, NW Argentina). *Earth and Planetary Science Letters*, 440,  
1191 33-42. <https://doi.org/10.1016/j.epsl.2016.02.009>, 2016.

1192 Pingel, H., Strecker, M.R., Alonso, R.N., Schmitt, A.K. Neotectonic basin and landscape evolution in  
1193 the Eastern Cordillera of NW Argentina, Humahuaca Basin (~ 24 S). *Basin Research*, 25(5),  
1194 554-573. <https://doi.org/10.1111/bre.12016>, 2013.

1195 Placzek, C., Quade, J., Patchett, P.J. Geochronology and stratigraphy of late Pleistocene lake cycles on  
1196 the southern Bolivian Altiplano: implications for causes of tropical climate change. *Geological  
1197 Society of America Bulletin*, 118(5-6), 515-532. <https://doi.org/10.1130/B25770.1>, 2006.

1198 Prush, V.B., Oskin, M.E. A mechanistic erosion model for cosmogenic nuclide inheritance in single-  
1199 clast exposure ages. *Earth and Planetary Science Letters* 535, 116066.  
1200 <https://doi.org/10.1016/j.epsl.2020.116066>, 2020.

1201 Ratnayaka, K., Hetzel, R., Hornung, J., Hampel, A., Hinderer, M., Frechen, M. Postglacial alluvial fan  
1202 dynamics in the Cordillera Oriental, Peru, and palaeoclimatic implications. *Quaternary  
1203 Research*, 91, 431–449. <https://doi.org/10.1017/qua.2018.106>, 2019.

1204 Robinson, R.A.J., Spencer, J.Q.G., Strecker, M.R., Richter, A., Alonso, R.N. Luminescence dating of  
1205 alluvial fans in intramontane basins of NW Argentina. In: Harvey, A.M. et. al, eds. *Alluvial  
1206 Fans: Geomorphology, Sedimentology, Dynamics*. Geological Society. Special Publication  
1207 251, 153-168. 2005.

1208 Rohais, S., Bonnet, S. and Eschard, R. Sedimentary record of tectonic and climatic erosional  
1209 perturbations in an experimental coupled catchment-fan system. *Basin Research*, 24(2), 198-  
1210 212. <https://doi.org/10.1111/j.1365-2117.2011.00520.x>, 2012.

- 1211 Savi, S., Tofelde, S., Wickert, A.D., Bufe, A., Schildgen, T.F., Strecker, M.R. Interactions between  
 1212 main channels and tributary alluvial fans: channel adjustments and sediment-signal  
 1213 propagation. *Earth Surface Dynamics*, 8(2), 303-322. [https://doi.org/10.5194/esurf-8-303-](https://doi.org/10.5194/esurf-8-303-2020)  
 1214 [2020](https://doi.org/10.5194/esurf-8-303-2020), 2020.
- 1215 Savi, S., Schildgen, T.F., Tofelde, S., Wittmann, H., Scherler, D., Mey, J., Alonso, R.N., Strecker, M.R.  
 1216 Climatic controls on debris-flow activity and sediment aggradation: The Del Medio fan, NW  
 1217 Argentina. *Journal of Geophysical Research: Earth Surface* 121, 2424–2445.  
 1218 <https://doi.org/10.1002/2016JF003912>, 2016.
- 1219 Schildgen, T.F., Robinson, R.A.J., Savi, S., Phillips, W.M., Spencer, J.Q.G., Bookhagen, B., Scherler,  
 1220 D., Tofelde, S., Alonso, R.N., Kubik, P.W., Binnie, S.A., Strecker, M.R. Landscape response  
 1221 to late Pleistocene climate change in NW Argentina: Sediment flux modulated by basin  
 1222 geometry and connectivity. *Journal of Geophysical Research: Earth Surface* 121, 392–414.  
 1223 <https://doi.org/10.1002/2015JF003607>, 2016.
- 1224 Schwab, K., Schäfer, A. Sedimentation und Tektonik im mittleren Abschnitt des Río Toro in der  
 1225 Ostkordillere NW-Argentiniens. *Geologische Rundschau*, 65, 175-194.  
 1226 <https://doi.org/10.1007/BF01808462>, 1976.
- 1227 Schwanghart, W., Scherler, D. Short Communication: TopoToolbox 2 – MATLAB-based software for  
 1228 topographic analysis and modeling in Earth surface sciences. *Earth Surface Dynamics* 2, 1–7.  
 1229 <https://doi.org/10.5194/esurf-2-1-2014>, 2014.
- 1230 Simpson, G., Castellort, S. Model shows that rivers transmit high-frequency climate cycles to the  
 1231 sedimentary record. *Geology* 40, 1131–1134. <https://doi.org/10.1130/G33451.1>, 2012.
- 1232 Seagren, E.G., Schoenbohm, L.M. Drainage reorganization across the Puna Plateau margin (NW  
 1233 Argentina): Implications for the preservation of orogenic plateaus. *Journal of Geophysical  
 1234 Research: Earth Surface*, 126(8), p.e2021JF006147. <https://doi.org/10.1029/2021JF006147>,  
 1235 2021.
- 1236 Seagren, E.G., McMillan, M., Schoenbohm, L.M. Tectonic control on drainage evolution in broken  
 1237 forelands: Examples from NW Argentina. *Tectonics*, 41(1), p.e2020TC006536,  
 1238 <https://doi.org/10.1029/2020TC006536>, 2022.
- 1239 Spelz, R.M., Fletcher, J.M., Owen, L.A. and Caffee, M.W. Quaternary alluvial-fan development,  
 1240 climate and morphologic dating of fault scarps in Laguna Salada, Baja California,  
 1241 Mexico. *Geomorphology*, 102(3-4), 578-594.  
 1242 <https://doi.org/10.1016/j.geomorph.2008.06.001>, 2008.
- 1243 Steffen, D., Schlunegger, F., Preusser, F. Late Pleistocene fans and terraces in the Majes valley,  
 1244 southern Peru, and their relation to climatic variations. *International Journal of Earth  
 1245 Sciences*, 99, 1975-1989. <https://doi.org/10.1007/s00531-009-0489-2>, 2010.
- 1246 Sternai, P., Herman, F., Valla, P.G., Champagnac, J.D. Spatial and temporal variations of glacial erosion  
 1247 in the Rhône valley (Swiss Alps): Insights from numerical modeling. *Earth and Planetary  
 1248 Science Letters* 368, 119–131. <https://doi.org/10.1016/j.epsl.2013.02.039>, 2013.
- 1249 Stone, J.O. Air pressure and cosmogenic isotope production. *Journal of Geophysical Research: Solid  
 1250 Earth* 105, 23753–23759. 2000.
- 1251 Strecker, M.R., Alonso, R., Bookhagen, B., Carrapa, B., Coutand, I., Hain, M.P., Hilley, G.E.,  
 1252 Mortimer, E., Schoenbohm, L., Sobel, E.R., 2009. Does the topographic distribution of the  
 1253 central Andean Puna Plateau result from climatic or geodynamic processes? *Geology*, 37(7),  
 1254 643-646. <https://doi.org/10.1130/G25545A.1>, 2009.
- 1255 Streit, R.L., Burbank, D.W., Strecker, M.R., Alonso, R.N., Cottle, J.M., Kylander-Clark, A.R.C.  
 1256 Controls on intermontane basin filling, isolation and incision on the margin of the Puna Plateau,  
 1257 NW Argentina (~23°S). *Basin Research* 29, 131–155. <https://doi.org/10.1111/bre.12141>, 2017.
- 1258 Terrizzano, C.M., García Morabito, E., Christl, M., Likerman, J., Tobal, J., Yamin, M., Zech, R.  
 1259 Climatic and Tectonic forcing on alluvial fans in the Southern Central Andes. *Quaternary  
 1260 Science Reviews* 172, 131–141. <https://doi.org/10.1016/j.quascirev.2017.08.002>, 2017.
- 1261 Tobal, J.E., Morabito, E.G., Terrizzano, C.M., Zech, R., Colavitto, B., Struck, J., Christl, M., Ghiglione,  
 1262 M.C. Quaternary landscape evolution of Patagonia at the Chilean Triple Junction: Climate and  
 1263 tectonic forcings. *Quaternary Science Reviews*, 261, 106960.  
 1264 <https://doi.org/10.1016/j.quascirev.2021.106960>, 2021.

- 1265 Tofelde, S., Duesing, W., Schildgen, T.F., Wickert, A.D., Wittmann, H., Alonso, R.N., Strecker, M.  
1266 Effects of deep-seated versus shallow hillslope processes on cosmogenic <sup>10</sup>Be concentrations  
1267 in fluvial sand and gravel. *Earth Surface Processes and Landforms* 43, 3086–3098.  
1268 <https://doi.org/10.1002/esp.4471>, 2018.
- 1269 Tofelde, S., Savi, S., Wickert, A.D., Bufo, A., Schildgen, T.F. Alluvial channel response to  
1270 environmental perturbations: Fill-terrace formation and sediment-signal disruption. *Earth*  
1271 *Surface Dynamics* 7, 609–631. <https://doi.org/10.5194/esurf-7-609-2019>, 2019.
- 1272 Tofelde, S., Schildgen, T.F., Savi, S., Pingel, H., Wickert, A.D., Bookhagen, B., Wittmann, H., Alonso,  
1273 R.N., Cottle, J., Strecker, M.R. 100 kyr fluvial cut-and-fill terrace cycles since the Middle  
1274 Pleistocene in the southern Central Andes, NW Argentina. *Earth and Planetary Science Letters*  
1275 473, 141–153. <https://doi.org/10.1016/j.epsl.2017.06.001>, 2017.
- 1276 Uppala, S.M., Kållberg, P.W., Simmons, A.J., Andrae, U., Bechtold, V.D.C., Fiorino, M., Gibson, J.K.,  
1277 Haseler, J., Hernandez, A., Kelly, G.A., Li, X., Onogi, K., Saarinen, S., Sokka, N., Allan, R.P.,  
1278 Andersson, E., Arpe, K., Balmaseda, M.A., Beljaars, A.C.M., Berg, L. Van De, Bidlot, J.,  
1279 Bormann, N., Cairns, S., Chevallier, F., Dethof, A., Dragosavac, M., Fisher, M., Fuentes, M.,  
1280 Hagemann, S., Hólm, E., Hoskins, B.J., Isaksen, I., Janssen, P.A.E.M., Jenne, R., McNally,  
1281 A.P., Mahfouf, J.-F., Morcrette, J.-J., Rayner, N.A., Saunders, R.W., Simon, P., Sterl, A.,  
1282 Trenberth, K.E., Untch, A., Vasiljevic, D., Viterbo, P., Woollen, J. The ERA-40 re-analysis.  
1283 *Quarterly Journal of the Royal Meteorological Society* 131, 2961–3012.  
1284 <https://doi.org/10.1256/qj.04.176>, 2005.
- 1285 Valla, P.G., Shuster, D.L., Van Der Beek, P.A. Significant increase in relief of the European Alps during  
1286 mid-Pleistocene glaciations. *Nature Geoscience*, 4(10), 688–692.  
1287 <https://doi.org/10.1038/ngeo1242>, 2011.
- 1288 van den Berg, van Saparoea, A.-P. H., Postma, G. Control of climate change on the yield of river  
1289 systems, Recent Adv. Model. Siliciclastic Shallow-Marine Stratigr. SEPM Spec. Publ., 90, 15–  
1290 33, 2008, <https://doi.org/10.2110/pec.08.90.0015>
- 1291 Ventra, D., Nichols, G.J. Autogenic dynamics of alluvial fans in endorheic basins: outcrop examples  
1292 and stratigraphic significance. *Sedimentology*, 61(3), 767–791.  
1293 <https://doi.org/10.1111/sed.12077>, 2014.
- 1294 Vera, C., Higgins, W., Amador, J., Ambrizzi, T., Garreaud, R., Gochis, D., Gutzler, D., Lettenmaier,  
1295 D., Marengo, J., Mechoso, C.R., Nogues-Paegle, J. Toward a unified view of the American  
1296 monsoon systems. *Journal of Climate*, 19(20), 4977–5000. <https://doi.org/10.1175/JCLI3896.1>,  
1297 2006.
- 1298 Vezzoli, L., Acocella, V., Omarini, R., Mazzuoli, R. Miocene sedimentation, volcanism and  
1299 deformation in the Eastern Cordillera (24°30' S, NW Argentina): Tracking the evolution of the  
1300 foreland basin of the Central Andes. *Basin Research* 24, 637–663.  
1301 <https://doi.org/10.1111/j.1365-2117.2012.00547.x>, 2012.
- 1302 Vizy, E.K., Cook, K.H. Relationship between Amazon and high Andes rainfall. *Journal of Geophysical*  
1303 *Research: Atmospheres*, 112(D7). <https://doi.org/10.1029/2006JD007980>, 2007.
- 1304 von Blanckenburg, F., T. Hewawasam, and P. W. Kubik (2004), Cosmogenic nuclide evidence for  
1305 low weathering and denudation in the wet, tropical highlands of Sri Lanka, *Journal of*  
1306 *Geophysical Research-Earth Surface*, 109(F3), <https://doi.org/10.1029/2003jf000049>.
- 1307 Wang, X., Auler, A.S., Edwards, R.L., Cheng, H., Ito, E., Wang, Y., Kong, X., Solheid, M. Millennial-  
1308 scale precipitation changes in southern Brazil over the past 90,000 years. *Geophysical Research*  
1309 *Letters* 34 (23). <https://doi.org/10.1029/2007GL031149>, 2007.
- 1310 Wickert, A.D., Schildgen, T.F. Long-profile evolution of transport-limited gravel-bed rivers. *Earth*  
1311 *Surface Dynamics*, 7(1), 17–43. <https://doi.org/10.5194/esurf-7-17-2019>, 2019.
- 1312 Wittmann, H., Malusà, M.G., Resentini, A., Garzanti, E., Niedermann, S. The cosmogenic record of  
1313 mountain erosion transmitted across a foreland basin: Source-to-sink analysis of in situ <sup>10</sup>Be,  
1314 <sup>26</sup>Al and <sup>21</sup>Ne in sediment of the Po river catchment. *Earth and Planetary Science Letters* 452,  
1315 258–271. <https://doi.org/10.1016/j.epsl.2016.07.017>, 2016.
- 1316 Zech, J., Terrizzano, C.M., Garcia Morabito, E., Veit, H., Zech, R. Timing and extent of late Pleistocene  
1317 glaciation in the arid Central Andes of Argentina and Chile (22°–41°S). *CIG* 43(2):697-  
1318 718. <http://dx.doi.org/10.18172/cig.3235>, 2017.

1319 Zondervan, J.R., Stokes, M., Boulton, S.J., Telfer, M.W., Mather, A.E. Rock strength and structural  
1320 controls on fluvial erodibility: Implications for drainage divide mobility in a collisional  
1321 mountain belt. *Earth and Planetary Science Letters*, 538, 116221.  
1322 <https://doi.org/10.1016/j.epsl.2020.116221>, 2020.  
1323